Title: **A genome wide CRISPR screen reveals novel determinants of long-lived plasma cell secretory capacity**

Authors: Lucas J. D'Souza[1], Jonathan N. Young[2,3], Heather Coffman[2], Edward P. Petrow Jr.[4], and Deepta Bhattacharya[1]

Affiliations: [1]Department of Immunobiology, University of Arizona, Tucson, AZ; [2]Department of Otolaryngology, University of Arizona, Tucson, AZ; [3]Current Address: Sutter Medical Foundation, Sacramento, CA; [4]Tucson Orthopedic Institute, Tucson, AZ.

Address correspondence to deeptab@arizona.edu

Summary: Long-lived plasma cells rely on V-type ATPases, PI4K, DDX3X, and MYD88 signals for maximal secretory capacity and survival

Abstract

Plasma cell subsets vary in their lifespans and ability to sustain humoral immunity. We conducted a genome-wide CRISPR-Cas9 screen in myeloma cells for factors that promote surface expression of CD98, a marker of longevity in mouse plasma cells. A large fraction of genes found to promote CD98 expression in this screen are involved in secretory and other vesicles, including subunits of the V-type ATPase complex. Genetic ablation and chemical inhibition of V-type ATPases in myeloma cells and primary plasma cells, respectively, reduced antibody secretion. Mouse and human long-lived plasma cells had greater numbers of acidified vesicles than their short-lived counterparts, and this correlated with increased antibody secretory capacity. The screen also revealed a requirement for the signaling adapter MYD88 in CD98 expression. Plasma cell-specific deletion of *Myd88* led to reduced survival and antibody secretion by antigen-specific cells *in vivo* and unresponsiveness to BAFF and APRIL *ex vivo*. These data reveal novel regulators that link plasma cell secretory capacity and lifespan.

Introduction

The humoral response following infection or vaccination involves recognition and activation of B cells by cognate antigen, followed by expansion, selection, and differentiation of these cells into quiescent memory B cells and antibody secreting plasma cells. If these antibodies are specific for protective epitopes on the pathogen, even small quantities can protect against otherwise lethal infections (Purtha et al., 2011). Thus, maintenance of protective antibody production is a key aspect of durable immunity. Yet, antibody production following some vaccines and infections are stable over time whereas others do so more transiently (Amanna et al., 2007; Olsson et al., 2007; Olotu et al., 2013; White et al., 2015). Underlying this variability is the lifespan of plasma cells that are generated.

Plasma cell subsets of varying longevity can be distinguished by using a combination of phenotypic markers. Human long-lived plasma cells tend to lack expression of CD19 (Mei et al., 2015; Halliley et al., 2015), though there are some exceptions to this rule (Brynjolfsson et al., 2017; Nguyen et al., 2024). In mice, a combination of markers such as BLIMP1 expression, B220, CD93, CXCR3, MHC-II, SLAMF6, LAG3, and the uptake of the fluorescent compound 2-deoxy-2-[(7-Nitro-2,1,3-benzoxadiazol-4-yl)-amino]-D-glucose (2NBDG) define plasma cell subsets of varying lifespans (D'Souza and Bhattacharya, 2019; Robinson et al., 2023; Lam et al., 2018; D'Souza et al., 2022). Another marker is the solute carrier protein CD98, which on the cell surface is subtly more highly expressed by long-lived plasma cells relative to their shorter-lived counterparts (Lam et al., 2018). CD98 is a heterodimer comprised of a

49 heavy chain encoded by the *Slc3a2* gene and a light chain by the *Slc7a5* gene
50 (Yanagida et al., 2001). This covalent pairing is not exclusive as the SLC3A2 protein can
51 heterodimerize with other members of the SLC7 family to form a variety of transporters
52 involved in amino acid uptake (Cantor and Ginsberg, 2012). Besides importing amino
53 acids, CD98 can also interact with integrin β subunits to facilitate cell growth and
54 survival (Feral et al., 2005). In plasma cells, the transcription factor BLIMP1 directly
55 promotes *Slc7a5* expression (Tellier et al., 2016).

56 The activity of BLIMP1 is a major defining factor for inducing antibody secretory
57 capacity in plasma cells. It does so in three distinct ways: first, by inducing a robust
58 increase in transcription of *Igh* and *Igl* transcripts in plasma cells (Minnich et al., 2016);
59 second, by upregulating the elongation factor ELL2 that permits alternative processing
60 of the 3' end of *Igh* transcripts and enabling translation of secretion-specific
61 immunoglobulin heavy-chain proteins (Martincic et al., 2009); and lastly by inducing
62 ATF4, ATF6, and XBP1 expression to support the high rate of antibody synthesis and
63 folding as well as expansion of the ER network and secretory apparatus necessary for
64 secretion (Tellier et al., 2016; Reimold et al., 2001; Shaffer et al., 2004; Hu et al., 2009;
65 Taubenheim et al., 2012). Aside from BLIMP1, mTORC1 signaling is another key
66 pathway that promotes antibody secretion (Jones et al., 2016; Benhamron et al., 2015;
67 Brookens et al., 2020).

68 There is conflicting evidence of whether antibody secretory capacity and plasma
69 cell lifespan are related or independent. On one hand, deletion of the transcription factor
70 XBP-1 sharply reduces antibody secretory capacity but does not impact plasma cell

71 differentiation or survival (Taubenheim et al., 2012). Similarly, genetic ablation of mTOR
72 signaling in plasma cells reduces secretory capacity but not survival (Jones et al., 2016).
73 These data demonstrate that there is no absolute requirement of antibody secretion for
74 plasma cell survival. On the other hand, long-lived plasma cells tend to secrete more
75 antibodies on a per cell basis than do their short-lived counterparts, but expression of
76 XBP-1 and mTOR signaling are similar across these subsets (Lam et al., 2018). It
77 therefore remains possible that some common pathways tune both lifespan and
78 secretory capacity, perhaps explaining some of the functional heterogeneity in plasma
79 cells. To identify such pathways, we performed an unbiased loss-of-function screen for
80 genes that promote CD98 expression and investigated their roles in plasma cell function
81 and longevity.

82 **Results**

83 *CD98 expression on plasma cells correlates with 2NBDG uptake and is independent of*
84 *secreted antibody isotype*

85 We first characterized markers of plasma cell longevity that could potentially be
86 used in genome-wide screens. In previous work, we showed that 2NBDG uptake
87 correlated with the longevity of plasma cell subsets (Lam et al., 2018; D'Souza and
88 Bhattacharya, 2019). Plasma cells that were 2NBDG+ also showed slightly higher levels
89 of the large neutral amino acid transporter CD98, which is composed of SLC3A2 and
90 SLC7A5, relative to their 2NBDG- counterparts. To test if immunoglobulin isotype usage
91 impacts these correlations, we injected C57BL/6 (B6) mice with 2NBDG and enriched
92 for CD138+ cells from spleens and bone marrow. A large fraction of splenic CD138+
93 B220+/- plasma cells were IgM+ while IgA+ plasma cells made up less than 10% of the
94 pool **(Fig. S1 A)**. Consistent with previous reports and in contrast to the spleen (Wilmore
95 et al., 2018), bone marrow plasma cells were mostly IgM+ or IgA+ **(Fig. S1 B)**. IgA+
96 plasma cells showed the highest frequency of 2NBDG+ cells followed by IgM+, and then
97 IgG+ or IgE+ plasma cells in both spleen and bone marrow **(Fig. S1 C)**. When matched
98 for antibody isotype, surface CD98 mean fluorescence intensity (MFI) was higher in
99 plasma cells that took up 2NBDG (LLPCs) relative to plasma cells that were 2NBDG-
100 (SLPCs) **(Fig. 1 A-C)**. Bone marrow LLPCs showed higher CD98 levels relative to their
101 splenic counterparts. To quantify total, rather than just surface CD98 protein levels, we
102 purified SLPCs and LLPCs from the spleens and bone marrows of B6 mice and
103 examined for expression of CD98 following fixation and permeabilization. Again, bone

104 marrow LLPCs had the highest total expression of CD98, followed by splenic LLPCs and
105 then splenic SLPCs **(Fig. 1 D)**. Consistent with these findings, we used imaging flow
106 cytometry to observe CD98 on both the surface and within the cytosol of fixed and
107 permeabilized plasma cells in all groups **(Fig. 1 E)**. Bone marrow LLPCs showed the
108 highest levels of CD98 on their surface as measured by similarity morphology indexes
109 with CD138 as compared to both splenic plasma cell populations **(Fig. 1 E)**.

110 Transcript abundances of *Slc3a2* and *Slc7a5*, as measured by RNA sequencing
111 (Lam et al., 2018), were similar across plasma cell subsets **(Fig. 1 F)**. Transcript reads of
112 *Prdm1*, which encodes for BLIMP-1, a known regulator of CD98 levels in plasma cells
113 (Shi et al., 2015; Tellier et al., 2016), were also similar between short- and long-lived
114 subsets **(Fig. 1 G)**. Thus, the differences between CD98 expression are apparent across
115 plasma cell subsets irrespective of isotype and do not appear to be regulated at the
116 level of transcription.

117

118 *A genetic screen to identify factors required for CD98 expression*

119 In prior CRISPR approaches, we were unsuccessful in identifying genes that
120 promote 2NBDG uptake (D'Souza et al., 2022). Given that elevated CD98 also marks
121 long-lived plasma cell subsets, we carried out an unbiased genome wide CRISPR
122 knockout screen for genes that promote its expression. We engineered the mouse
123 myeloma cell line, 5TGM1, to express a Doxycycline inducible version of Cas9 (5TGM1-
124 iCas9) **(Fig. S2 A)**. This strategy was chosen to allow for expansion of cells containing

125 gRNAs that target essential genes which might otherwise have been lost in a constitutive
126 Cas9 expression system. We then transduced 5TGM1-iCas9 cells with the Brie library
127 containing 78,637 gRNAs targeting 19,674 genes of the mouse genome (Doench et al.,
128 2016). After transduction, gRNAs were represented at levels similar to the input plasmid
129 library (r^2=0.57, **Fig. S2 B)**. We induced Cas9 expression by adding Doxycycline to the
130 cell culture media and incubated cells for 7 days to ablate genes and promote complete
131 depletion of residual proteins. From the Doxycycline treated cultures, we then sorted
132 cells with reduced CD98 expression by FACS to purities >95% **(Fig. 2 A)**. Genomic DNA
133 was then extracted from these cells and gRNA sequences amplified by PCR from the
134 CD98-low and the total 5TGM1-iCas9-Brie populations. The resultant amplicons were
135 sequenced and the abundance of gRNA was quantified relative to the total cell fraction
136 using the Model-based Analysis of Genome-wide CRISPR/Cas9 Knockout (MaGeCK)
137 algorithm (Li et al., 2014).

138 In the CD98-low fraction, we observed 34 genes targeted by the gRNAs with
139 greater than 2-fold enrichment and with a false discovery rate <0.05 **(Fig. 2 D)**. We
140 observed enrichment of gRNAs targeting *Slc3a2* and *Slc7a5*, the genes that encode the
141 heavy and light chains of the CD98 heterodimer, providing internal validation of the
142 results of the genome-wide screen. Among the remaining significant 32 gRNA-targeted
143 genes, we found 8 genes that associate with endosomal vesicles and 8 members of the
144 vesicle-associated V-type ATPase complex. The remaining 16 genes include those that
145 encode RNA export and processing proteins (*Thoc3*, *Ddx3x*, *Nob1*, *RnaseK*, and
146 *Rbm33*), signaling intermediates (*Myd88*, *Myc*, and *Pi4kb*), proteins involved in genome

147 structure (*Rad21* and *Smc3*), and the chaperone *Hsp90b1*. We did not identify *Prdm1* as
148 a hit, despite its known role in promoting CD98 expression (Tellier et al., 2016). Yet
149 when we compared cells treated with Doxycycline to untreated controls at day 7, we
150 observed a drop in the read counts for gRNAs targeting *Irf4*, *Prdm1*, *Xbp1*, *Atf4*, and
151 *Atf6b*, indicating a selection against cells that deleted these genes and potentially
152 limiting their detection in our screen **(Fig. S2 C)**.

153

154 *Long-lived plasma cells have higher frequencies of acidic vesicles than do short-lived*
155 *plasma cells*

156 Given the enrichment of genes involved in multiple vesicular components and V-
157 type ATPases in the screen, we chose to focus on these pathways first. The V-type
158 ATPase is a multi-protein complex composed of a membrane bound proton pump (V0)
159 powered by a cytosol-facing subunit (V1) that hydrolyzes ATP (Collins and Forgac,
160 2020). It acidifies lysosomes, endosomes, Golgi complexes, and secretory vesicles, all of
161 which have significantly lower luminal pH relative to the cytosol (Casey et al., 2010). We
162 purified mouse plasma cell subsets by FACS and quantified the frequencies of acidic
163 vesicles using intracellular staining and imaging cytometry. Total ATP6V1A+ spot
164 numbers per cell were slightly higher in bone marrow LLPCs relative to splenic LLPCs
165 and SLPCs **(Fig. 3 A)**. To identify vesicular content differences more specifically
166 between plasma cell subsets, we used characteristic markers. RAB7+ endosomes were
167 present at higher frequencies in LLPCs of both spleen and bone marrow compared to

168 SLPCs **(Fig. 3 B)**. Further, LAMP1+ lysosome frequencies per cell were highest in bone
169 marrow LLPCs, followed by splenic LLPCs and SLPCs **(Fig. 3 C)**. We next examined if
170 human plasma cell populations demonstrated similar trends for endosome and
171 lysosome frequencies (gated as in **Fig. S3**). We observed higher frequencies of
172 ATP6V1A+ and LAMP1+ vesicles in bone marrow plasma cells relative to tonsillar
173 plasma cells **(Fig. 3 D-E)**. Put together, the frequencies of acidic vesicles in plasma cells
174 are higher in subsets with longer lifespans.

175 We reasoned that these differences in vesicular content might reflect differential
176 antibody secretory capacities of plasma cell subsets. We sorted polyclonal SLPCs and
177 LLPCs from the spleens and bone marrows of mice and seeded equal numbers for
178 ELISpot assays, as spot size can serve as a surrogate of antibody secretory capacity
179 (Jones et al., 2016). We found that bone marrow LLPCs yielded spots with the largest
180 average area as compared to their splenic equivalents irrespective of antibody isotype
181 **(Fig. 4 A-D)**. Splenic SLPC spots were the smallest in comparison. Similarly,
182 irrespective of isotype, we found that human CD19- bone marrow plasma cells secreted
183 more antibodies per cell than did CD19+ bone marrow plasma cells **(Fig. 4 E-H)**, which
184 on an average have shorter lifespans than their CD19- counterparts. These findings
185 suggest that for both mice and humans and across isotypes, long-lived plasma cells
186 have higher numbers of acidic vesicles and secrete more antibodies than their shorter-
187 lived counterparts.

188

189 *Ablation of V-type ATPase function reduces antibody secretion*

190 We next addressed if there were a direct link between vesicular pH and the
191 antibody secretion capacity of plasma cells. In the first approach, we chemically
192 inhibited V-type ATPase activity using Bafilomycin A1 (Bowman et al., 1988). To detect
193 changes in vesicular pH in cells, we transduced Cas9-expressing 5TGM1 cells (5TGM1-
194 Cas9) with the pH Lysosomal Activity Reporter (pHLARE) construct (Webb et al., 2021).
195 The resultant 5TGM1-Cas9-pHLARE cells express *R. norvegicus* LAMP1 as a fusion
196 protein with the pH-sensitive superfolder GFP (sfGFP) in the lumen of the lysosome and
197 the pH-insensitive mCherry on the cytosol side of the lysosome, allowing for ratiometric
198 calculation of lysosomal pH (Pédelacq et al., 2006). We observed a 1.3- to 5.6-fold
199 increase in the ratio of sfGFP to mCherry in these cells with increasing concentrations of
200 Bafilomycin A1 **(Fig. 5 A)**. Reciprocally, the MFI of surface CD98 was proportionally
201 reduced in all groups treated with Bafilomycin A1 **(Fig. 5 B)**. Culture supernatants from
202 groups treated with higher doses of the inhibitor showed reduced antibody levels
203 relative to untreated controls **(Fig. 5 C)**. Lastly, we treated purified plasma cell subsets
204 with this inhibitor and observed a reduction in the spot size of secreted immunoglobulin
205 per cell **(Fig. 5 D)**. These findings indicate that pharmacological inhibition of V-type
206 ATPase activity impairs both surface CD98 expression and antibody secretion.

207 We confirmed these findings genetically by ablating V-type ATPase activity in
208 5TGM1 cells using CRISPR-Cas9. We targeted *Atp6v0b* and *Atp6v1a* as representative
209 genes of the V0 and V1 subunit of the ATPase complex. Targeting these genes led to a
210 nearly two-fold increase in the ratio of sfGFP to mCherry, indicating a rise in lysosomal

211 pH **(Fig. 5 E)**. This increase in sfGFP fluorescence can be traced to increased sfGFP
212 intensity on mCherry+ spots in cells as observed by imaging cytometry **(Fig. 5 F)**. In
213 both cases, we observed a drop in surface CD98 levels as well as secreted antibodies in
214 their culture supernatants **(Fig. 5 G-H)**. Further, the survival of *Atp6v0b*- and *Atp6v1a*-
215 deficient myeloma cells in culture was compromised relative to control cells **(Fig. S4)**. In
216 conclusion, V-type ATPases promote CD98 expression, survival, and antibody secretory
217 capacity of plasma cells.

218

219 *Pi4kb promotes vesicular acidification and antibody secretion in plasma cells*

220 Among the genes enriched in the CD98-low fraction was *Pi4kb*, the gene that
221 encodes the enzyme phosphatidylinositol-4-hydroxide kinase B (PI4KB). It is a type-III
222 PI4K that catalyzes the formation of phosphoinositide-4-phosphate (PI4P) at Golgi
223 surfaces which subsequently promotes vesicle formation (Meyers and Cantley, 1997;
224 Godi et al., 1999; Baba and Balla, 2020). We ablated *Pi4kb* in 5TGM1-Cas9 cells using
225 CRISPR-Cas9 and observed a drop in the total numbers of ATP6V1A+ spots per cell
226 and LAMP1+ lysosomes per cell **(Fig. 6 A-B)**. Deletion of *Pi4kb* in 5TGM1-Cas9-
227 pHLARE cells showed lysosomes with higher sfGFP signal **(Fig. 6 C)**, suggesting that
228 loss of PI4KB leads to poor maintenance of V-type ATPase complexes and vesicular
229 acidification. *Pi4kb*-deficient 5TGM1 cells also showed reduced surface CD98
230 expression, secreted fewer antibodies, and had poor survival in culture **(Fig. 6 D-E and**

231 **Fig. S4)**. Thus, PI4KB promotes the formation and acidification of intracellular vesicles
232 and antibody secretory capacity through V-type ATPase function.

233

234 *DDX3X affects antibody secretory capacity of plasma cells independent of vesicular*
235 *acidification*

236 The ATP-dependent DEAD-box RNA helicase *Ddx3x* was another highly enriched
237 gene in the CD98-low fraction **(Fig. 2 B)**. The DDX3X protein associates with complex
238 secondary structures in mRNA and enables protein synthesis (Lai et al., 2008; Soto-Rifo
239 et al., 2012; Calviello et al., 2021). Deletion of *Ddx3x* in 5TGM1-Cas9 cells reduced
240 surface CD98 levels and decreased secreted immunoglobulin in culture supernatants
241 **(Fig. 7 A-B)**. Ablating *Ddx3x* expression in 5TGM1-Cas9-pHLARE cells did not affect
242 lysosomal pH levels, suggesting that it regulates the antibody secretory capacity of cells
243 through a mechanism distinct from the PI4KB-V-type ATPase pathway **(Fig. 7 C)**.
244 *Ddx3x*-deficient myeloma cells also survived poorly in culture over time **(Fig. S4)**. We
245 next lentivirally transduced 5TGM1-Cas9 cells with wild-type human DDX3X (hsDDX3X)
246 or versions with point mutations in their helicase domain (T323I, R326H) or aberrations
247 in their ATP-binding domain (I415Δ, T532M) that have previously been reported in
248 patients with DDX3X syndrome (Lennox et al., 2020). We then depleted murine wild-
249 type DDX3X in these cells using a gRNA that targeting mouse *Ddx3x* but not the
250 transgenic hs*Ddx3x* cassette. At 5 days post-transduction, we found that deleted
251 cultures were rescued by unmodified hsDDX3X (WT) as measured by surface CD98

252 levels **(Fig. 7 D-E)**. When quantified by ELISA, these cultures also showed similar levels
253 of secreted immunoglobulin in their supernatants relative to untargeted control cells,
254 indicating that expression of hsDDX3X overcame the defect otherwise seen with
255 ablation of endogenous DDX3X **(Fig. 7 F)**. In all cases, overexpression of hsDDX3X
256 mutants failed to rescue surface CD98 levels or secreted immunoglobulin in culture
257 supernatants **(Fig. 7 D-F)**. This observation is not because of differential levels of
258 DDX3X overexpression, as they were found to be comparable across all groups when
259 probed for intracellular DDX3X protein **(Fig. S5)**. Put together, both the ATPase and
260 helicase domain of DDX3X are necessary for proper antibody secretion in plasma cells.

261

262 *MYD88 is a plasma cell intrinsic determinant of antibody secretion capacity*

263 We observed an enrichment of gRNAs targeting the signaling intermediate
264 MYD88 in the CD98-low fraction **(Fig. 2 B)**. MYD88 is an adaptor protein required for
265 transducing signals through all Toll-like receptors (TLRs), the IL-1 receptor (IL-1R), and
266 cytokine signals through Transmembrane Activator and CAMI Interactor (TACI) by
267 TRAF6-dependent and -independent mechanisms (Takeda and Akira, 2004). As *Myd88*-
268 germline knockout (KO) mice are viable and do not show any defects in B cell
269 development (Pasare and Medzhitov, 2005), we first examined plasma cell subsets for
270 CD98 expression. We injected *Myd88*-KO and age- and sex-matched C57BL/6N mice
271 with 2NBDG and examined plasma cell subsets from the spleens and bone marrows of
272 these mice. Across all 2NBDG-subsets, *Myd88*-KO plasma cells had lower expression of

273 surface CD98 **(Fig. 8 A)**. We then seeded equal numbers of plasma cell subsets into an
274 ELISpot assay. As signals downstream of MYD88 promote class-switch recombination
275 (He et al., 2010), we compared only IgM-expressing plasma cell subsets. IgM+ spot
276 areas were reduced only in splenic and bone marrow LLPCs, suggesting that MYD88
277 signals promote antibody secretion in longer-lived plasma cell subsets **(Fig. 8 B)**.

278 To test if MYD88 affects antibody secretory capacity in a plasma cell intrinsic
279 manner, we generated lineage specific *Myd88* knockout mice. We bred mice with loxP
280 sites flanking exon 3 of the *Myd88* genomic locus (*Myd88* fl/fl) with mice carrying an
281 IRES-CreERT2 cassette at the 3' UTR of the *IgJ* locus (Jchain-CreERT2). In these mice,
282 treatment with tamoxifen induces deletion of *Myd88* in plasma cells without impacting
283 other cell types (Hou et al., 2008; Wong et al., 2020). We immunized these mice (Jchain-
284 CreERT2+/- *Myd88* fl/fl) along with littermate Cre-negative (Jchain-CreERT2-/- *Myd88*
285 fl/fl) and Cre-only (Jchain-CreERT2+/-) control mice with 100μg NP-CGG in 1%
286 Alhydrogel, an adjuvant that does not activate TLR signals (Gavin et al., 2006). At 8
287 weeks, we observed comparable levels of serum NP-specific antibodies across all
288 groups **(Fig. 8 C)**. We then fed mice Tamoxifen chow over the course of 2 weeks to
289 induce deletion of *Myd88*. Bone marrow LLPCs from these treated mice were then
290 enriched and examined for spot frequencies and sizes in ELISpot assays. We observed
291 a significant reduction in both the numbers and spot sizes of NP-specific plasma cells in
292 the bone marrows of Jchain-CreERT2+/- *Myd88* fl/fl mice relative to both control mouse
293 groups **(Fig. 8 D-E)**. This suggests that plasma cell intrinsic MYD88 signaling promotes
294 both survival and secretory capacity of plasma cells *in vivo*.

295 *Cytokine signals through TACI calibrate antibody secretory capacity in a MYD88 fashion*

296 To identify which MYD88-dependent signals promote antibody secretion, we
297 examined a previously generated RNAseq databases for expression of receptors that
298 signal through MYD88 in plasma cells and myeloma cells (Lam et al., 2018; D'Souza et
299 al., 2022). We observed no detectable levels of *Il1r* transcript in all populations
300 examined, but high expression of *Tnfrsf13b*, the gene that encodes TACI, in all groups
301 **(Fig. S6 A)**. Further, we observed elevated expression of TACI on long-lived *ex vivo*
302 plasma cells relative to short-lived ones **(Fig. S6 B)**. Though primary plasma cells
303 express multiple TLR family members, 5TGM1 cells only expressed TLR4 **(Fig. S6 C)**.
304 We therefore ablated *Tnfrsf13b*, *Tlr4*, *Myd88*, and *Traf6* (the gene that encodes TRAF6,
305 a downstream molecule of the MYD88 cascade) in 5TGM1 myeloma cells using
306 CRISPR-Cas9. Ablation of each of these genes resulted in reduced surface CD98 and
307 fewer antibodies in culture supernatants relative to cells transduced with a control gRNA
308 **(Fig. 9 A-B)**. To test if signaling through TACI and TLR ligands promote antibody
309 secretion in *ex vivo* plasma cells, we treated purified short- and long-lived plasma cells
310 from B6 mice with the High Mobility Group Box 1 (HMGB1) protein, a known
311 endogenous ligand of TLRs (Yu et al., 2010), or B-cell Activating Factor (BAFF) or A
312 Proliferation-inducing ligand (APRIL), known ligands of TACI, and measured secretory
313 capacity in ELISpot assays. In parallel, we treated plasma cell subsets from *Myd88*-KO
314 mice with the aforementioned ligands. Exogenous HMGB1 did not impact antibody
315 secretion in any of the plasma cell subsets examined **(Fig. 9 C)**. Addition of BAFF or
316 APRIL, however, increased the spot size of longer-lived plasma cells relative to

317 untreated groups and had minimal impact on short-lived plasma cells **(Fig. 9 D-E)**. This
318 effect on antibody secretion was MYD88-dependent, as these cytokines had no effect
319 on plasma cells from *Myd88*-KO mice. Thus, APRIL and BAFF signal through TACI and
320 MYD88 to influence the antibody secretory capacity of long-lived plasma cells.

321 **Discussion**

322 Plasma cell subsets vary in their lifespans and presumably their ability to sustain
323 durable humoral immunity. Subtle differences in CD98 expression distinguish these
324 subsets, thereby providing a convenient handle for unbiased genome-wide screens for
325 factors that promote plasma cell longevity. We identified 34 genes that included a
326 variety of vesicular proteins, subunits of the V-type ATPase complex, RNA export and
327 processing proteins, and various signaling factors that promote CD98 expression.
328 Though the original intent of the screen was to identify determinants of lifespan, all of
329 the factors we tested impacted secretory capacity. These data suggest some
330 convergence in factors that fine tune plasma cell lifespan and antibody secretion.

331 Nearly half of the genes identified in our screen encode proteins associated with
332 intracellular vesicles and acidification. The vesicular network is relevant to plasma cells
333 to support the secretory capacity and high rate of translation, folding, and antibody
334 production in these cells (Casey et al., 2010). The frequency of acidic vesicles was
335 higher in longer-lived plasma cell subsets relative to their short-lived counterparts,
336 consistent with their elevated antibody secretory capacity. Impeding RAB7 exchange
337 with RAB5 on endosomes inhibited antibody secretion and plasma cell longevity,
338 demonstrating the importance of endosomal function in plasma cells (Pone et al., 2015;
339 Lam et al., 2016). The greater numbers of acidic vesicles in long-lived plasma cells
340 compared to short-lived plasma cells likely depend on the activity of the inositol kinase
341 PI4KB, which has been shown in multiple systems to promote lysosomal integrity,
342 vesicle formation, and retention of integral proteins to these organelles like the V-type

343 ATPase complexes (Balla et al., 2002; Sridhar et al., 2013). The factors that might
344 promote differential PI4KB activity in plasma cell subsets are currently unknown.

345 Our data further reveals the complex regulation of antibody secretion in plasma
346 cells by identifying a role for the RNA helicase DDX3X in modulating this process. This
347 protein has been shown to associate with secondary structures at the 5' end of mRNA
348 and unwinds them through its helicase activity, allowing for recruitment of ribosomes
349 and its subsequent translation (Calviello et al., 2021; Shih et al., 2008). In plasma cells,
350 this function is particularly relevant as DDX3X activity might ease barriers in mRNA
351 translation and support a steady rate of antibody synthesis and secretion. While it is
352 likely that DDX3X associates with *Igh* and *Igl* mRNA due to their sheer abundance in
353 plasma cells (Shi et al., 2015), identifying transcripts bound to DDX3X in plasma cells
354 might provide insights to the translational regulation of key proteins for cellular function.
355 As mice with lymphocyte-specific ablation of *Ddx3x* show reductions in B cell numbers
356 (Szappanos et al., 2018; Liu et al., 2018), generating inducible models of *Ddx3x* deletion
357 may help us understand the role of this factor in plasma cell longevity. Further, as males
358 express a homolog of DDX3X called DDX3Y, it would be interesting to observe if the two
359 factors have overlapping targets in plasma cells from males and compensate for each
360 other in the absence of one or the other (Sekiguchi et al., 2004).

361 While MYD88 has been well-studied in B cells, our report demonstrates a plasma
362 cell intrinsic role for this signaling intermediate in modulation CD98 expression, survival,
363 and antibody secretion. We further demonstrate that BAFF and APRIL likely mediate
364 these effects through TACI and MYD88, but not through interactions with their other

365 receptors, BAFF-R and BCMA, both of which are MYD88-independent (He et al., 2010;
366 Smulski and Eibel, 2018). Signals through APRIL and its receptors are particularly
367 relevant in the bone marrow niche, where plasma cells are immersed in a milieu of
368 extracellular matrix proteins, cytokines, and cell adhesion factors that promote their
369 survival *in vivo* (Cassese et al., 2003; O'Connor et al., 2004; Belnoue et al., 2008;
370 Rozanski et al., 2011; Nguyen et al., 2018; Ishikawa et al., 2024). BAFF in turn has been
371 shown to be crucial for B cell survival and plasma cell differentiation (Avery et al., 2003;
372 Benson et al., 2008; Parsa et al., 2016). Our findings suggest that while APRIL can
373 promote plasma cell survival by interacting with both BCMA and TACI, and BAFF with
374 TACI and BAFF-R (Eslami et al., 2024), they can only enhance antibody secretion
375 through their interaction with TACI and subsequent signaling through MYD88. This data
376 also indicates that the secretory capacity of plasma cells is not exclusively a cell intrinsic
377 function but can be modulated by external stimuli.

378 CRISPR-Cas9 screens were recently carried out by multiple independent groups
379 to identify factors regulating plasma cell differentiation (Pinter et al., 2022; Xiong et al.,
380 2022) and antibody secretion (Trezise et al., 2023) using *in vitro* primary B cell systems.
381 Of the genes shown to be important for antibody secretion, such as those involved in
382 the unfolded protein response, we found little overlap with the genes in our dataset. This
383 may be due to our use of CD98 as a marker, which varies with antibody secretory
384 capacity across plasma cell subsets but not as a function of the unfolded protein
385 response (Lam et al., 2018). Our screen was thus more likely to identify pathways that
386 differ between plasma cell subsets than common pathways required for secretory

387 capacity. Put together, our data suggest there are distinct programs required for the
388 induction of antibody secretion: those that are absolutely required and used similarly
389 across plasma cell subsets, and others that further tune lifespan and secretory capacity.
390 At least some of the latter pathways functionally link survival and antibody secretion,
391 thereby allowing relatively few highly secretory long-lived plasma cells to provide robust
392 protection.

393

394 **Acknowledgements**

395 The authors wish to thank the flow cytometry core at the University of Arizona for their
396 assistance. The core is supported by RII of the University of Arizona and an NCI grant
397 P30CA023074. Use of the Imagestream was made possible by a NIH award S10
398 OD028466. We are also grateful to Colin Fields for his assistance in procuring human
399 samples after surgery and Jean Wilson, Hannah Pizzato, and Kit Tobey for their inputs.
400 We also wish to thank William Smith and the staff at University Animal Care for their
401 assistance with mouse husbandry and maintenance. This project was supported by a
402 NIH grant R01AI129945 to D.B. and a Bio5 postdoctoral fellowship to L.J.D. The funders
403 of this project had no role in study design, data collection and interpretation, decision to
404 publish, or composing the manuscript. There was no additional external funding
405 received for this study.

406

407 **Conflict of interest**

408 Sana Biotechnology has licensed intellectual property of D.B. and Washington University
409 in St. Louis. Inograft biotherapeutics and Jasper Therapeutics have licensed intellectual
410 property of D.B. and Stanford University. D.B. is on the scientific advisory board for
411 Hillevax. D.B. is a scientific co-founder of Aleutian Therapeutics. L.J.D, J.N.Y, H.C., and
412 E.P.P. report no conflict of interest.

413 **Materials and methods**

414 *Mice*

415 C57BL/6N mice (556) were purchased from the Charles River laboratories. *Myd88*-null
416 (9088) and *Myd88*-flox (8888) mice were purchased from Jackson Laboratories (Hou et
417 al., 2008). Jchain-CreERT2 mice have been generated previously (Wong et al., 2020).
418 Mice were housed and bred under specific pathogen free conditions. Experiments were
419 carried out on age- and sex-matched mice between 8-12 weeks in age. All animal
420 procedures were executed under the guidelines provided by the Institutional Animal
421 Ethics committee of the University of Arizona. Euthanasia was carried out by carbon
422 dioxide asphyxiation at the rate of 1.8-4.0 L/minute in a 7L chamber until 1 minute after
423 respiration ceased. Mice were then cervically dislocated to ensure death. For some
424 experiments, mice sedated with Fluriso (Vet One) were injected intravenously with
425 100µg of 2NBDG (Cayman Chemical company) and euthanized after 20 minutes.

426 *Human tissues*

427 Tonsil samples were obtained from consenting adults undergoing elective
428 tonsillectomies (Banner-University Medical Center). Bone marrow samples were
429 obtained from persons undergoing robotics-assisted hip arthroplasty (Tucson
430 Orthopedic Institute). All donors were anonymous, and no patient data was collected as
431 part of this investigation. All human work was conducted in accordance with federal,
432 state, and county regulations and approved by the University of Arizona IRB.

433 *Immunizations*

434 Mice were immunized intraperitoneally with 100µg NP-CGG (Biosearch Technologies) in
435 1% Alhydrogel (Invivogen). Circulating blood was collected by venipuncture of the tail
436 vein from immunized mice and allowed to stand at room temperature to coagulate
437 overnight. Serum was collected after spinning down the samples at 15000rpm for 10
438 minutes. At 8 weeks post-immunization, mice were fed special chow containing 400mg
439 Tamoxifen citrate per kg diet (Envigo) for two weeks prior to euthanasia.

440 *Primary cells*

441 Single cell suspensions of spleens were prepared by macerating organs with frosted
442 slides while bone marrow cells were isolated from tibiae, fibulae, femurs, and pelvic
443 bones using a mortar and pestle in 1x PBS containing 5% Adult bovine serum (MP
444 Biomedical; hereon referred to as FACS buffer). Human tonsils were sliced using a
445 scalpel and forceps and ground in FACS buffer using a mortar and pestle. Human bone
446 marrow reamings were shaken vigorously in a sterile container containing FACS buffer.
447 In all cases, cells were filtered through a 70-micron nylon mesh to remove debris. Single
448 cell suspensions were treated in an ammonium chloride-potassium (ACK) hypotonic
449 lysis solution to lyse erythrocytes followed by density gradient centrifugation on a
450 Histopaque-1119 layer (Millipore Sigma). To enrich for murine plasma cells, whole cell
451 suspensions were enriched by labelling with an appropriate anti-CD138 antibody
452 (Biolegend) followed by anti-APC or anti-PE microbeads and enriched using LS columns
453 (all from Miltenyi Biotec). CD38+ tonsil and bone marrow cells were enriched similarly
454 from whole cell suspensions. For some experiments, CD38-enriched cells were
455 cryopreserved in 50% incomplete RPMI (Thermo Fisher Scientific), 40% fetal calf serum

456 (Peak Serum), and 10% DMSO (Millipore Sigma) until the time of experimentation. For
457 intracellular staining, cells were first fixed with 2% Paraformaldehyde (Electron
458 microscopy services) for 10 minutes followed by permeabilization with 0.1% Saponin
459 (Millipore Sigma).

460 *Plasmids*

461 The mouse Brie CRISPR-knockout library (73633), lentiGuide-puro (52963), pLenti-
462 sfGFP-LAMP1-mCherry (164478), and pHAGE-DDX3X (116730) were all purchased
463 from Addgene (Doench et al., 2016; Sanjana et al., 2014; Webb et al., 2021; Ng et al.,
464 2018). The lentiGuide-mCherry plasmid (217005) was generated in-house (D'Souza et
465 al., 2022). Edit-R inducible lentiviral hEF1α-Blast-Cas9 nuclease plasmid (CAS11229)
466 was purchased from Dharmacon. Guide RNA (gRNA) targeting genes of interest were
467 chosen from the Brie CRISPR-knockout library and cloned into an empty lentiGuide-
468 puro construct as described previously (D'Souza et al., 2022). Mouse genomic *Ddx3x*-
469 specific gRNA were designed using CRISPick (Doench et al., 2016; Sanson et al., 2018).
470 pMD2.G (12259) and psPAX2 (12260) were used to generate lentivirus and were also
471 purchased from Addgene. T323I, R326H, I415Δ, and T532M mutations were introduced
472 into the parental pHAGE-DDX3X by PCR and site-directed mutagenesis using the KLD
473 enzyme reaction (New England Biolabs). Positive mutants were identified by Sanger
474 sequencing (Eton Biosciences). Plasmids were transformed and grown in XL-1 Blue
475 cells (Agilent Technologies) or *Stbl4* competent cells (Thermo Fisher Scientific) for
476 plasmids larger than 10kb.

477 *Cell lines and cell culture*

478 The 5TGM1 myeloma line was a kind gift from Michael H. Tomasson while at
479 Washington University in St. Louis (Garrett et al., 1997). 5TGM1 cells expressing a
480 Doxycyline-inducible Cas9 (5TGM1-iCas9) was generated by transducing cells with
481 lentivirus containing the Edit-R inducible Cas9 construct at 2500rpm for 90 minutes at
482 room temperature followed by culturing cells in media containing 10µg/mL Blasticidin-
483 HCl (Thermo Fisher Scientific). Cells were sorted into single cell clones by FACS and
484 screened for lines not expressing Cas9 in regular doxycycline-free media. 5TGM1 cells
485 expressing Cas9 constitutively (5TGM1-Cas9) were generated previously (D'Souza et
486 al., 2022). These cells were transduced with lentivirus containing the pHLARE cassette
487 by spin-infection and positive cells were FACS-sorted as GFP+ mCherry+ cells.
488 Overexpression constructs for human DDX3X and mutants were introduced into
489 5TGM1-Cas9 cells similarly and purified based on GFP expression. All 5TGM1 lines
490 were cultured in RPMI (Gibco) containing 10% FBS, 1mM Sodium pyruvate, 2mM
491 GlutaMAX, 10µg/mL Ciprofloxacin-HCl, minimum-essential amino acids, Penicillin and
492 Streptomycin (hereon referred to as cRPMI). After introduction of gRNA constructs, cells
493 were incubated for 5 days at 37°C with 5% CO_2. For antibody secretion assays, 100,000
494 5TGM1 cells were seeded in triplicates into wells of a 96-well plated and incubated
495 overnight. Culture supernatants were harvested the next day and assayed for secreted
496 immunoglobulins. Where indicated, cells were treated with Bafilomycin A1 (Millipore
497 Sigma) at varying concentrations. For some experiments, cells were treated with
498 10µg/mL mouse HMGB-1 (ACRO Biosystems), 10ng/mL recombinant mouse BAFF

499 (R&D Systems), or 10ng/mL recombinant mouse APRIL (Thermo Fisher Scientific).
500 Lenti-X 293T cells were purchased from Takara and cultured in DMEM (Cytiva) with all
501 the additional supplements described previously for RPMI. Lentivirus were generated
502 from these cells by transient transfection of plasmids with packaging constructs
503 previously complexed with GeneJuice (Millipore Sigma).

504 *Flow cytometry*

505 Single cell preparations were stained with the following antibodies from Biolegend: anti-
506 mouse CD138-PE, -APC, or -BV510 (281-2); anti-mouse B220-AlexaFluor700 (RA3-
507 6B2); anti-mouse CD98-AlexaFluor647 or -PE-Cy7 (4F2); anti-human CD38-PE (HB-7);
508 anti-human CD27-APC (M-T271); anti-human CD19-BV421 (HIB19); anti-human IgM-
509 BV650 (MHM-88); anti-human CD138-FITC (MI15). Rat anti-mouse IgA-BV421 (C10-1)
510 was purchased from BD Biosciences. Goat F(ab')2 anti-human IgA-AlexaFluor647
511 (2052-31) was purchased from Southern Biotech. Unconjugated antibodies against
512 mouse/human ATP6V1A (EPR19270), RAB7 (EPR7589), and LAMP1 (ab24170) were all
513 purchased from Abcam and used at a 1:500 dilution. Stained organelles were detected
514 with an anti-rabbit IgG-AlexaFluor405 reagent (A48258, Thermo Fisher Scientific). Other
515 antibodies from Thermo Fisher Scientific used in this study are anti-mouse IgM-PerCP-
516 eFluor710 (II41), and anti-mouse/human DDX3X (A300-474A). Propidium iodide and
517 DAPI (both from Millipore Sigma), were used to stain dead cells in some assays. In some
518 experiments Zombie UV or Zombie Red (both from Biolegend) were used to stain dead
519 cells prior to fixation and permeabilization. Cells were analyzed for fluorescence on a BD
520 Fortessa cytometer (BD Biosciences) and data interpreted using the FlowJo software

521 (BD Biosciences). Intracellular organelle frequencies in cells were examined on an
522 Imagestream^{X} MkII (Cytek Biosciences) at 60x magnification with extended depth of
523 field. Spot numbers per cell and similarity morphology indexes were calculated on the
524 IDEAS software (Cytek Biosciences). Fluorescence associated cell sorting was carried
525 out on a FACS Aria II (BD Biosciences).

526 *Library screening and next generation sequencing*

527 The mouse Brie library was packaged into lentiviral particles by transient transfection of
528 Lenti-X 293T cells with the 5µg of the library plasmid, 1.75µg of pMD2.G and 3.25µg of
529 psPAX2 packaging constructs complexed with the GeneJuice transfection reagent
530 (Millipore Sigma). Culture supernatants were collected and pooled at 48h and 96h and
531 filtered through a 0.45µ syringe filter. Fresh filtered supernatants containing virus were
532 then used to transduce 5TGM1-iCas9 cells in the presence of 8µg of Polybrene
533 (Millipore Sigma). Positively transduced cells were then selected in cRPMI containing
534 Puromycin (Gibco). Cas9 expression in 40 million positively transduced 5TGM1-iCas9
535 cells (roughly 500x coverage of plasmid library) was induced after adding 300ng/mL
536 Doxycycline hyclate to culture media. After 7 days, cells were cultured with 10µg/mL of
537 2NBDG and then stained for surface CD98 expression. Live CD138+ CD98-low cells
538 were then FACS sorted into individual 15mL conical tubes. Genomic DNA from cells
539 were extracted using the mini genomic DNA extraction kit (IBI scientific) and gRNA
540 constructs amplified from it using Q5 Polymerase (New England Biolabs). Flow cell
541 attachment sequences, Illumina sequencing regions, and unique 3' barcode sequences
542 were then introduced by PCR. These pair-ended 150bp libraries were then sequenced

543 on a Novaseq 6000 (Illumina). FASTQ files containing 325-926 million reads were then
544 analyzed for gene enrichment in sorted fractions using the Python-based MaGeCK
545 module (Li et al., 2014). Representation of the Brie library in cells were confirmed by
546 comparing representation of gRNA from positively transduced cells to the parental Brie
547 library. Volcano plots showing enriched genes in sorted fractions relative to unenriched
548 cells were plotted using Prism v.10 (Graphpad).

549 *ELISA*

550 ELISA plates (Corning) were coated overnight at 4°C with unconjugated rat anti-mouse
551 κ-light chain (187.1, BD Biosciences) in a 0.1M Sodium carbonate-bicarbonate buffer
552 (pH: 9.5). The next day, plates were blocked with 2% Bovine Serum Albumin (Millipore
553 Sigma) in 1xPBS containing 0.05% Tween-20 (1xPBS-T) followed by incubation with
554 serial dilutions of cell-free culture supernatants. After 3 hours, plates were then washed
555 thrice with 1xPBS-T followed by an overnight incubation at 4°C with biotinylated rat anti-
556 mouse IgG2b (SB74g, Southern Biotech). Plates were washed the next day in 1xPBS-T
557 followed by an incubation with Streptavidin linked to horseradish peroxidase (BD
558 Biosciences) for an hour at room temperature. Plates were developed using a TMB
559 substrate (Alfa Aesar) and arrested with 2N Sulfuric acid (Millipore Sigma). Absorbance
560 was measured at 450nm and corrected for background absorbance at 650nm on a
561 VERSAmax microplate reader (Molecular devices). Area under the curve (AUC) was
562 calculated from background adjusted A450 values on the Prism v.10.3 (Graphpad). A
563 similar workflow was used for detection of NP-specific antibodies in serum, except that

564 ELISA plates were coated with NP_{10-19}-BSA (Biosearch technologies) and detected with
565 a Peroxidase-conjugated donkey anti-mouse IgG(H+L) (Jackson ImmunoResearch).

566 *ELISpot*

567 Multiscreen HTS HA filter plates (Millipore Sigma) were coated with NP-BSA (Biosearch
568 technologies), Goat anti-mouse Ig(H+L) (Southern Biotech), or a 1:1 mix of Goat anti-
569 human Lambda and Kappa (both from Southern Biotech) prepared in 1xPBS. After an
570 overnight incubation at 4°C, plates were blocked with RPMI containing 10% FBS at
571 37°C. Sorted cells were resuspended in cRPMI and seeded in triplicates in their
572 designated wells in the plate and incubated at 37°C overnight. Plates were washed the
573 next day with 1xPBS and then incubated overnight with the following peroxidase-
574 conjugated secondary reagents as appropriate: donkey anti-mouse IgG(H+L) for NP-
575 specific plasma cells (Jackson Immunoresearch); goat anti-mouse IgM (1020-05), anti-
576 IgG (1030-05), and anti-IgA (1040-05) for mouse splenic and bone marrow plasma cells;
577 goat anti-human IgM (2020-05), anti-IgG (2045-05), and anti-IgA (2050-05) for detection
578 of human bone marrow plasma cells (all from Southern Biotech). Spots were developed
579 using a TrueBlue Peroxidase substrate (Kirkegaard and Perry Laboratories) and washed
580 vigorously with MilliQ water. Spot size and numbers were quantified on the CTL
581 ImmunoSpot S6 analyzer. The total numbers of NP+ plasma cells were calculated by
582 multiplying the number of spots with the dilution factor and divided by total bone marrow
583 cell counts.

584 *Statistical analysis*

585 All statistical analysis was done using Prism v. 10.3 (Graphpad). Specific statistical tests
586 and significance are indicated in the figure legends of the indicated graphs. Fold
587 changes and p-values for the genome-wide screen were calculated by MaGeCK (Li et
588 al., 2014). Figure S2 A was generated using Biorender.

589

Figure 1

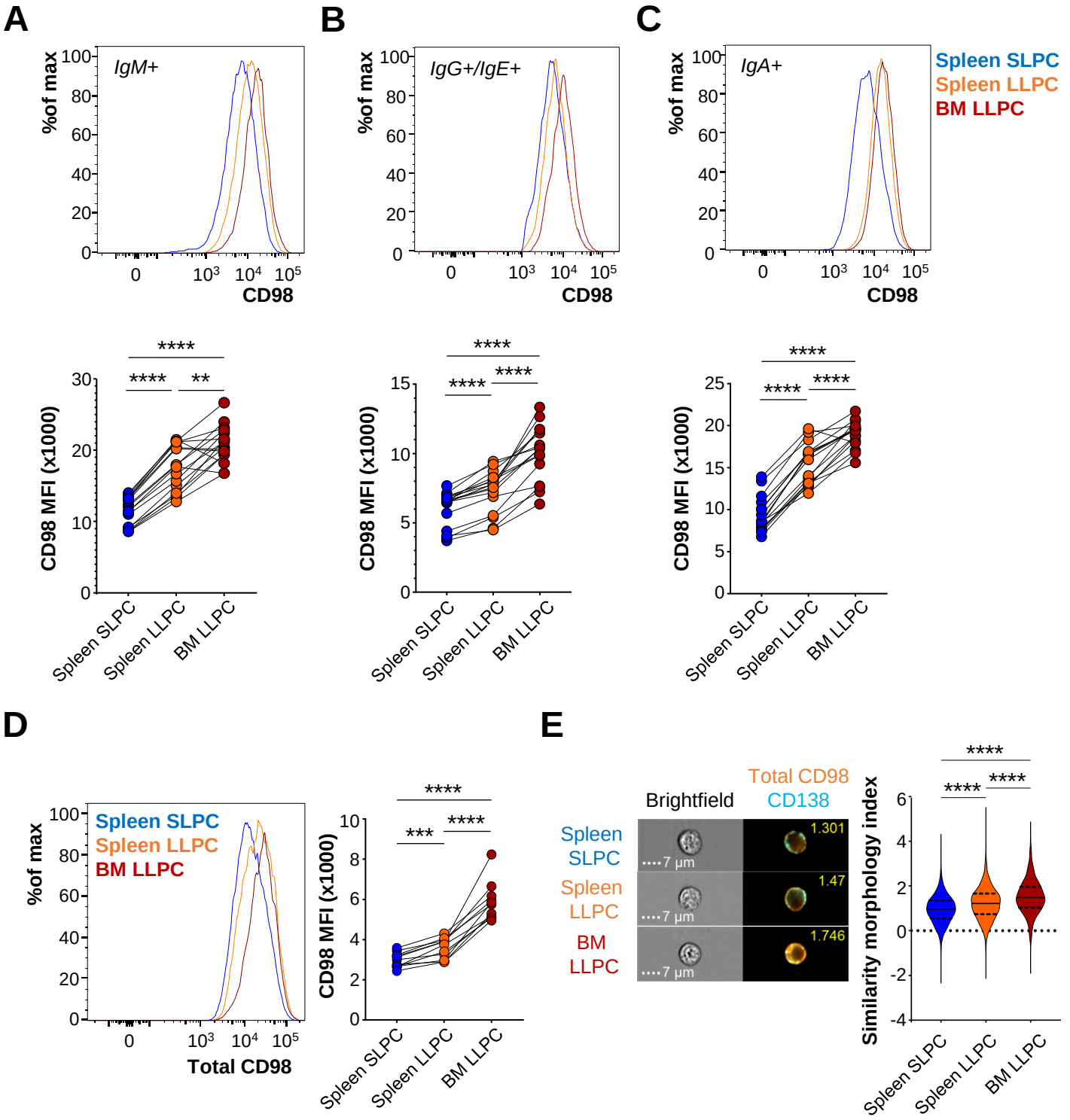
A
B
C
IgM+
IgG+/IgE+
IgA+
%of max
CD98
Spleen SLPC
Spleen LLPC
BM LLPC
CD98 MFI (x1000)
Spleen SLPC
Spleen LLPC
BM LLPC
D
E
Total CD98
Brightfield
CD138
Similarity morphology index
F
G
TPM
Slc3a2
Slc7a5
Prdm1

590 **Figure 1: LLPCs have higher levels of CD98 than SLPCs despite having similar**
591 **transcript reads**

592 **(A-C)** Representative histograms (top) and quantification of mean fluorescence intensity
593 (MFI) values (bottom) of CD98 expression on *ex vivo* (A) IgM+, (B) IgG+ and IgE+, and
594 (C) IgA+ plasma cell subsets. Each data point represents cells from one mouse, and
595 subsets from each mouse are connected by lines. Pooled data from 16 mice across 4
596 experiments. *p<0.05 by paired one-way ANOVA with Tukey's correction.

597 **(D)** Representative histogram of total (surface and internal) CD98 protein levels in
598 sorted plasma cell subsets (left). Quantification of total CD98 MFI of each subset is
599 represented (right). Each data point represents cells from one mouse, and subsets from
600 each mouse are connected by lines. Pooled data from 11 mice across 3 experiments.
601 *p<0.05 by paired one-way ANOVA with Tukey's correction.

602 **(E)** Cells in (D) were examined by imaging flow cytometry. Representative images for
603 each subset are shown with surface CD138 (cyan) and total CD98 (orange) and their
604 colocalization. Similarity morphology indices are indicated on the top right of the image
605 and values for each subset are quantified. Representative graph of one of three
606 independent experiments. *p<0.05 by unpaired one-way ANOVA with Games-Howell
607 corrections.

608 **(F)** Transcripts per million kilobase (TPM) values of CD98hc (*Slc3a2*) and CD98lc
609 (*Slc7a5*) from Lam WY *et al* (Cell Reports 2018), showing values across splenic and
610 bone marrow plasma cell subsets. Pooled data from three independent experiments.

611 **(G)** Transcripts per million kilobase (TPM) values for BLIMP1 (*Prdm1*) from Lam WY *et*

612 *al* (Cell Reports 2018) across splenic and bone marrow plasma cell subsets. Pooled data

613 from three independent experiments.

614

Figure 2

A

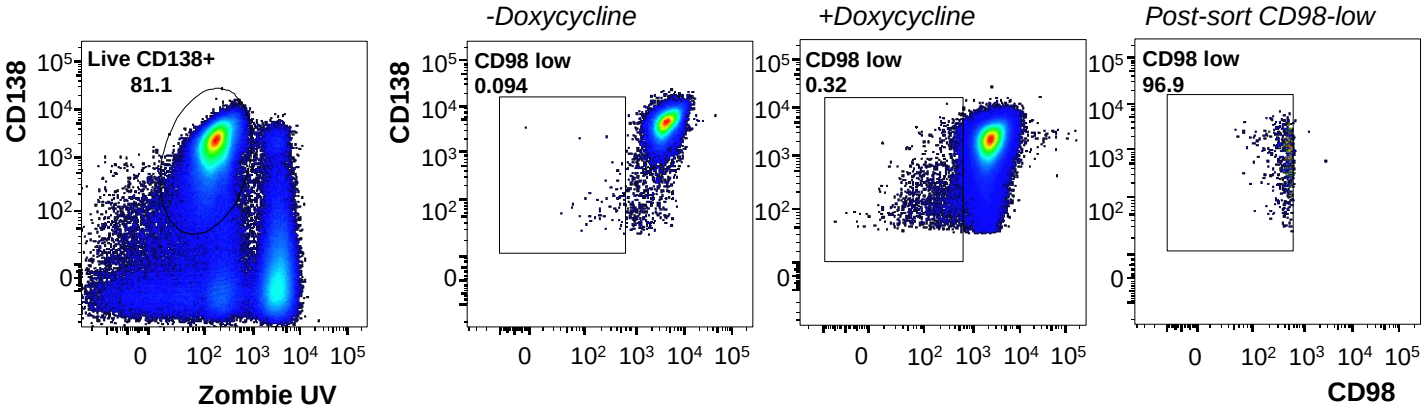

B

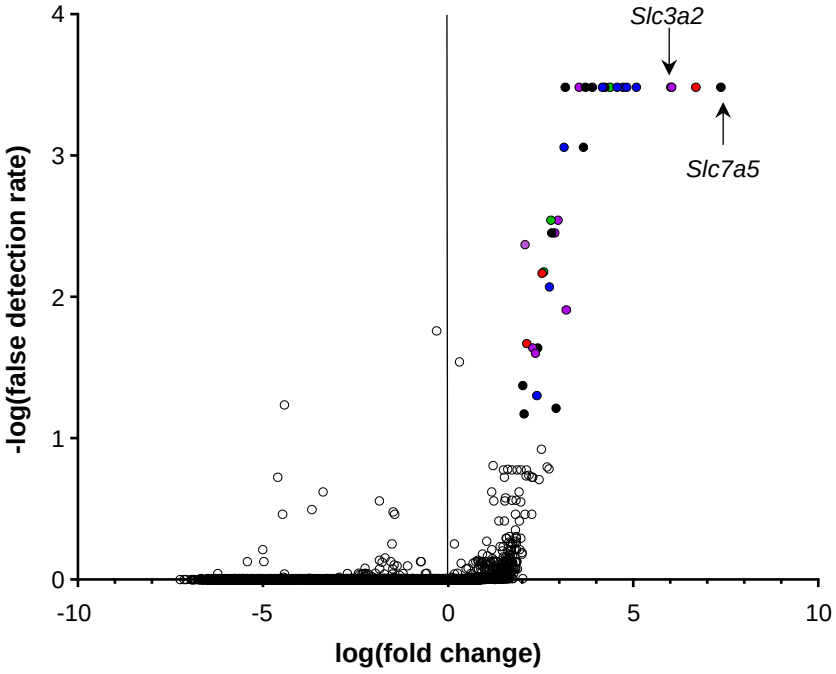

V-type ATPases
Atp6v0b
Atp6v0c
Atp6v0d1
Atp6v0e
Atp6v1a
Atp6v1b2
Atp6v1e1
Atp6v1g1

Vesicular proteins
Exoc5
Exoc8
Gosr2
Nsf
Scfd1
Stx4a
Trappc5
Trappc8

Signaling intermediates
Pi4kb
Myc
Myd88

RNA binding proteins
Ddx3x
Nob1
Rbm33
RnaseK

615 **Figure 2: Genes involved in vesicle biology and exocytosis promote plasma cell**
616 **CD98 expression**

617 **(A)** Representative gating on 5TGM1-iCas9 transduced with the mouse Brie gRNA
618 library. After treatment with Doxycycline for 7 days, 5TGM1-iCas9-Brie cells were gated
619 first to exclude dead cells and debris (far left). On this gate, cells were subsequently
620 gated as CD98-low based on the untreated 5TGM1-iCas9-Brie cells (center left). CD98-
621 low cells in Doxycycline treated cultures (center right) were then purified by FACS to
622 achieve a pure CD98-low fraction (far right).

623 **(B)** MAGeCK analysis of genes enriched in the CD98-low fraction relative to unsorted
624 5TGM1-iCas9 cells transduced with the Brie library. Volcano plot of fold change
625 between sorted cells against control cells are shown. Statistically significant genes are
626 indicated as filled circles, the color of which corresponds to the class of genes indicated
627 next to the volcano graph. Four biological replicates were analyzed.

628

Figure 3

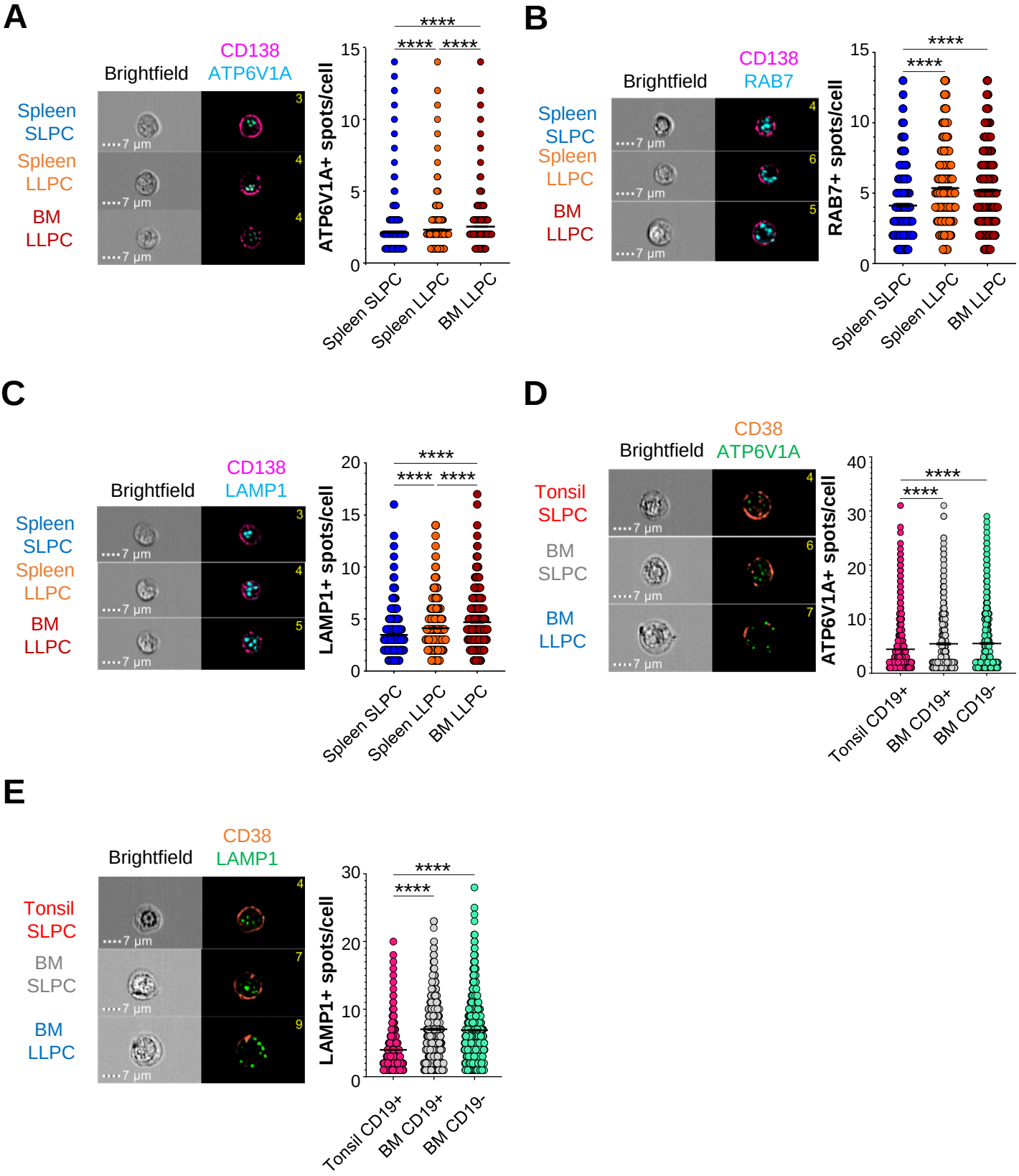
A
Brightfield
CD138
ATP6V1A
Spleen SLPC
Spleen LLPC
BM LLPC
7 µm
ATP6V1A+ spots/cell
Spleen SLPC
Spleen LLPC
BM LLPC
B
Brightfield
CD138
RAB7
RAB7+ spots/cell
C
Brightfield
CD138
LAMP1
LAMP1+ spots/cell
D
Brightfield
CD38
ATP6V1A
Tonsil SLPC
BM SLPC
BM LLPC
Tonsil CD19+
BM CD19+
BM CD19-
E
Brightfield
CD38
LAMP1
****

629 **Figure 3: LLPCs have higher frequencies of acidic vacuoles than SLPCs**

630 **(A)** Mouse plasma cell subsets from the spleen and bone marrow were sorted and
631 stained for surface CD138 (pink) and intracellular ATP6V1A protein (cyan) and cells
632 analyzed by imaging flow cytometry. Each circle represents one cell. ATP6V1A spot
633 numbers/cell were enumerated and mean +/- SEM shown. Combined data from 9890-
634 10755 cells from 12 mice across 3 experiments. *p<0.05 by unpaired one-way ANOVA
635 with Games-Howell corrections.

636 (**B)** Mouse plasma cell subsets as in (A) were stained for surface CD138 (pink) and
637 RAB7 (cyan). RAB7+ spot numbers/cell were enumerated and mean +/- SEM graphed.
638 Each circle represents one cell. Pooled data from 1639-2115 cells from 12 mice across
639 3 experiments. *p<0.05 by unpaired one-way ANOVA with Games-Howell corrections.

640 **(C)** Mouse plasma cell subsets as in (A) were stained for surface CD138 (pink) and
641 LAMP1 (cyan). LAMP1+ spot numbers/cell were enumerated and mean +/- SEM
642 graphed. Each circle represents one cell. Pooled data from 3061-9159 cells from 12
643 mice across 3 experiments. *p<0.05 by unpaired one-way ANOVA with Games-Howell
644 corrections.

645 **(D)** Human plasma cells from the tonsil (CD19+ CD38+ CD27+ CD138-) and bone
646 marrow CD19+ and CD19- plasma cells (CD27+ CD38+ CD138+) were stained for
647 surface CD38 (orange) and intracellular ATP6V1A protein. ATP6V1A+ spot numbers/cell
648 were quantified and mean +/- SEM plotted for all subsets. Each circle represents one
649 cell. Combined data from 1156-9050 cells from 7 tonsil donors and 6 bone marrow

650 donors across 3 experiments. *p<0.05 by unpaired one-way ANOVA with Games-Howell
651 corrections.

652 **(E)** Human plasma cell subsets as in (D) were stained for surface CD38 and intracellular
653 LAMP1. LAMP1+ spot numbers/cell were quantified and mean +/- SEM plotted. Each
654 circle represents one cell. Pooled data from 2614-10742 cells from 9 tonsil donors and 7
655 bone marrow donors from 4 experiments. *p<0.05 by unpaired one-way ANOVA with
656 Games-Howell corrections.

657

Figure 4

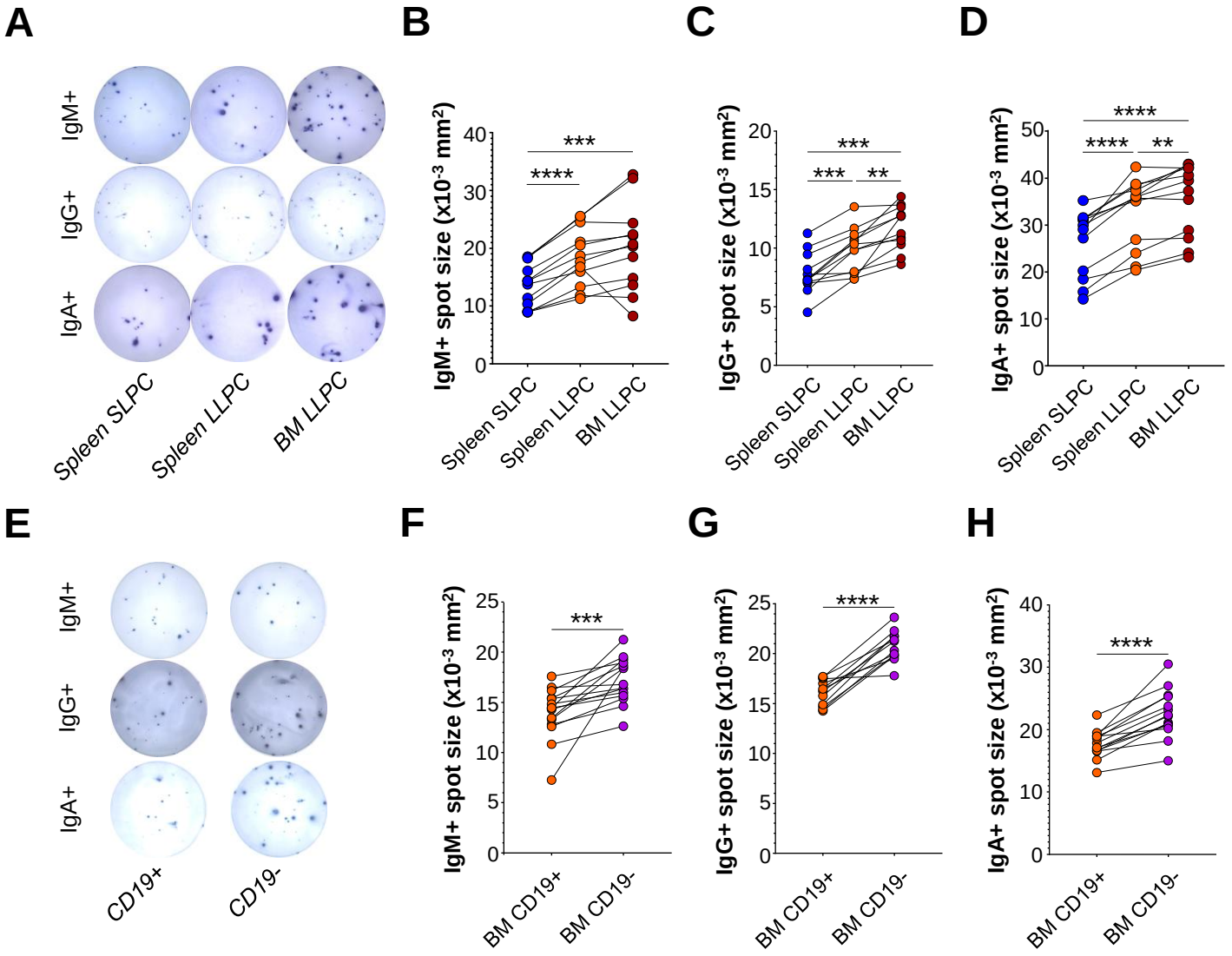
A
IgM+
IgG+
IgA+
Spleen SLPC
Spleen LLPC
BM LLPC
B
IgM+ spot size (x10-3 mm2)
***
****
C
IgG+ spot size (x10-3 mm2)
***
***
**
D
IgA+ spot size (x10-3 mm2)
****
****
**
E
IgM+
IgG+
IgA+
CD19+
CD19-
F
IgM+ spot size (x10-3 mm2)
***
G
IgG+ spot size (x10-3 mm2)
****
H
IgA+ spot size (x10-3 mm2)
****
BM CD19+
BM CD19-

658 **Figure 4: LLPCs secrete more antibodies than SLPCs independent of**

659 **immunoglobulin isotype**

660 **(A-D)** IgM+ *ex vivo* splenic SLPCs, LLPCs, and bone marrow LLPCs were sorted and
661 seeded into wells of an ELISpot plate. (A) Representative images showing spots for each
662 subset and isotype are indicated. Quantification of (B) IgM+, (C) IgG+, and (D) IgA+
663 plasma cell spot area of each subset is represented. Each data point represents mean
664 spot sizes from one mouse, and subsets within each mouse are connected by lines.
665 Pooled data from 12 mice across 3 experiments. *$p<0.05$ by paired one-way ANOVA
666 with Tukey's correction.

667 **(E-H)** Human bone marrow plasma cells (CD27+ CD38+ CD138+) were sorted as
668 CD19+ and CD19- populations and seeded into wells of an ELISpot plate. (E)
669 Representative images showing spots for CD19+/- plasma cells secreting the indicated
670 isotype are shown. Quantification of spot area of (F) IgM+, (G) IgG+, and (H) IgA+
671 plasma cells are represented. Each data point represents one donor, and subsets from
672 an individual are connected by lines. Pooled data from 15 donors across 4 experiments
673 for IgM, 12 donors across 3 experiments for IgG, and 14 donors across 4 experiments
674 for IgA. *$p<0.05$ by paired t tests.

675

Figure 5

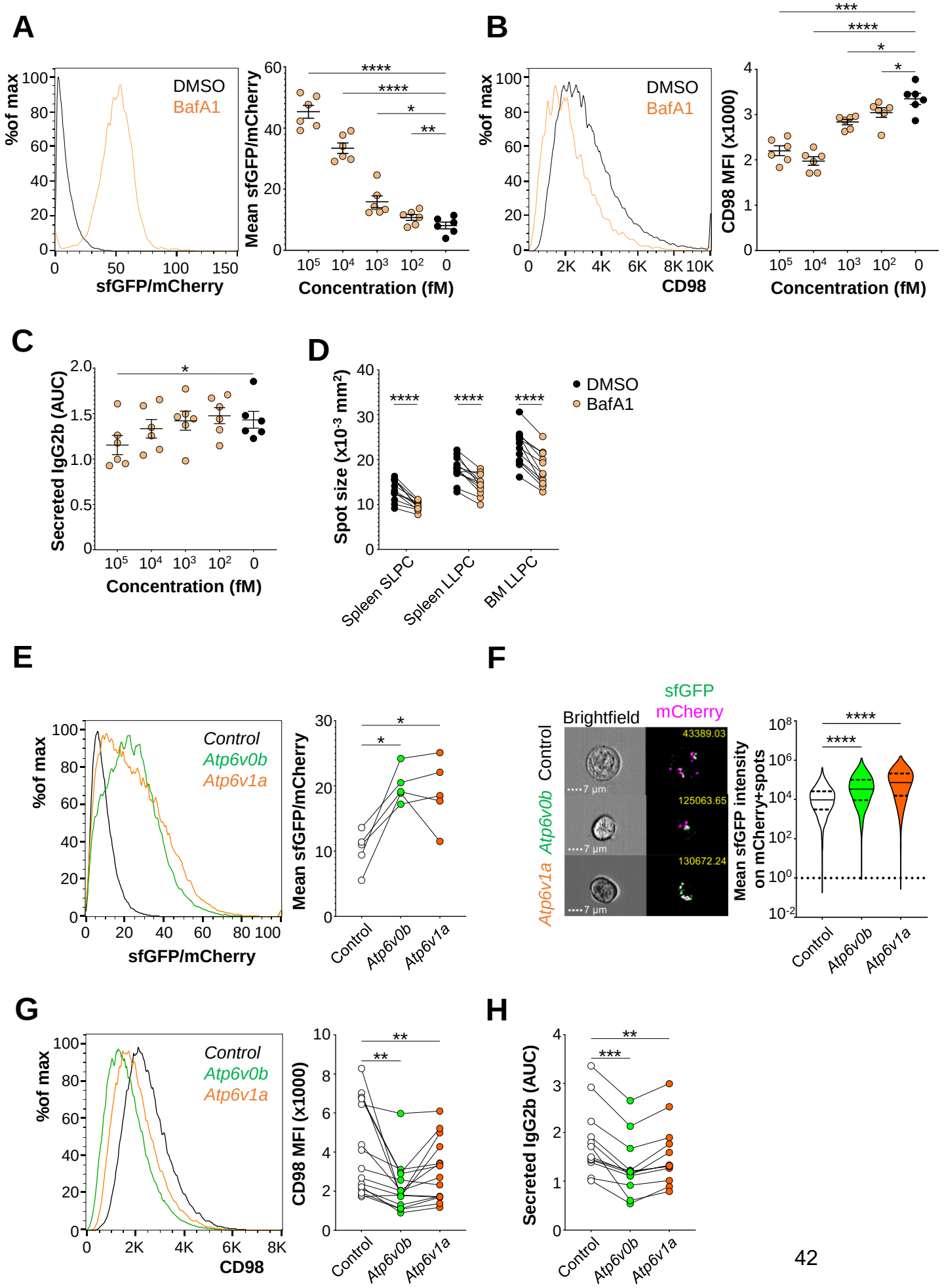
A
%of max
DMSO
BafA1
sfGFP/mCherry
Mean sfGFP/mCherry
Concentration (fM)
B
CD98 MFI (x1000)
CD98
C
Secreted IgG2b (AUC)
D
Spot size (x10⁻³ mm²)
Spleen SLPC
Spleen LLPC
BM LLPC
E
Control
Atp6v0b
Atp6v1a
F
Brightfield
sfGFP
mCherry
Mean sfGFP intensity on mCherry+spots
G
H

676 **Figure 5: V-type ATPase activity promotes CD98 expression and antibody**
677 **secretion**

678 **(A)** 5TGM1-Cas9-pHLARE cells were treated overnight with the indicated doses of
679 Bafilomycin A1. Representative histogram of the ratio of sfGFP to mCherry MFI in DMSO
680 (black) and 100nM Bafilomycin A1 (tan) treated groups (left). Quantification of mean
681 sfGFP/mCherry ratio (right) in control and knockout cultures is shown. Each circle
682 represents the MFI of cells in one well. Pooled data from 6 experiments. *$p<0.05$ by
683 repeated measures one-way ANOVA with Dunnett's correction.

684 **(B)** Cells in (A) were examined for MFI of surface CD98 by flow cytometry. Each circle
685 represents the mean values for cells from a single well of an experiment. Pooled data
686 from 6 experiments. *$p<0.05$ by repeated measures one-way ANOVA with Dunnett's
687 correction.

688 **(C)** Culture supernatants of cells in (A) were scored for secreted IgG2b by ELISA. AUC
689 for each group is shown. Pooled data from 6 independent experiments. *$p<0.05$ by
690 repeated measures one-way ANOVA with Dunnett's correction.

691 **(D)** *Ex vivo* plasma cell subsets were sorted, and equal numbers were seeded into wells
692 of an ELISpot plate containing media (untreated, black) or media with 10nM Bafilomycin
693 A1 (tan). Quantification of average spot area of each subset in each treatment is shown.
694 Each circle represents data from a single mouse and is connected across treatments
695 with a line. Pooled data from 12 mice from 3 experiments. *$p<0.05$ by two-way ANOVA.

696 **(E)** 5TGM1-Cas9-pHLARE cells were transduced with lentivirus containing gRNA
697 targeting *Atp6v0b* or *Atpv1a* along with a control gRNA. Representative histogram (left)
698 of the ratio of sfGFP to mCherry MFI in control gRNA (black), *Atp6v0b*- (green), and
699 *Atp6v1a*-targeting gRNA (orange) groups. Quantification of mean sfGFP/mCherry ratio
700 (right) in control and knockout cultures. Each circle represents a single treatment and
701 data points are joined by a line within the same experiment. Pooled data from 5
702 independent experiments. *p<0.05 by paired one-way ANOVA with Tukey's correction.

703 **(F)** Groups in (E) were assessed for sfGFP intensity on mCherry spots per cell by
704 imaging flow cytometry. Representative images of each group (left) at 60x are shown
705 with ratio values in the top right. Mean ratio of GFP intensity on mCherry+ spots/cell
706 were quantified. Each circle represents one cell from untreated/treated groups.
707 Representative graph of 3 independent experiments. *p<0.05 by unpaired one-way
708 ANOVA with Games-Howell corrections.

709 **(G)** CD98 expression on 5TGM1-Cas9 cells transduced with control gRNA (black),
710 *Atp6v0b*- (green), and *Atp6v1a*-targeting gRNA (orange). Representative histogram (left)
711 and quantified CD98 MFI (right) depicted. Each circle represents the MFI of cells in one
712 well and groups from the same experiment are connected by a line. Combined data
713 from 15 experiments. *p<0.05 by paired one-way ANOVA with Tukey's correction.

714 **(H)** Secreted IgG2b from culture supernatant of groups in (G) was quantified by ELISA.
715 Area under the curve (AUC) for each group is shown. Pooled data from 12 experiments.
716 *p<0.05 by paired one-way ANOVA with Tukey's correction.

Figure 6

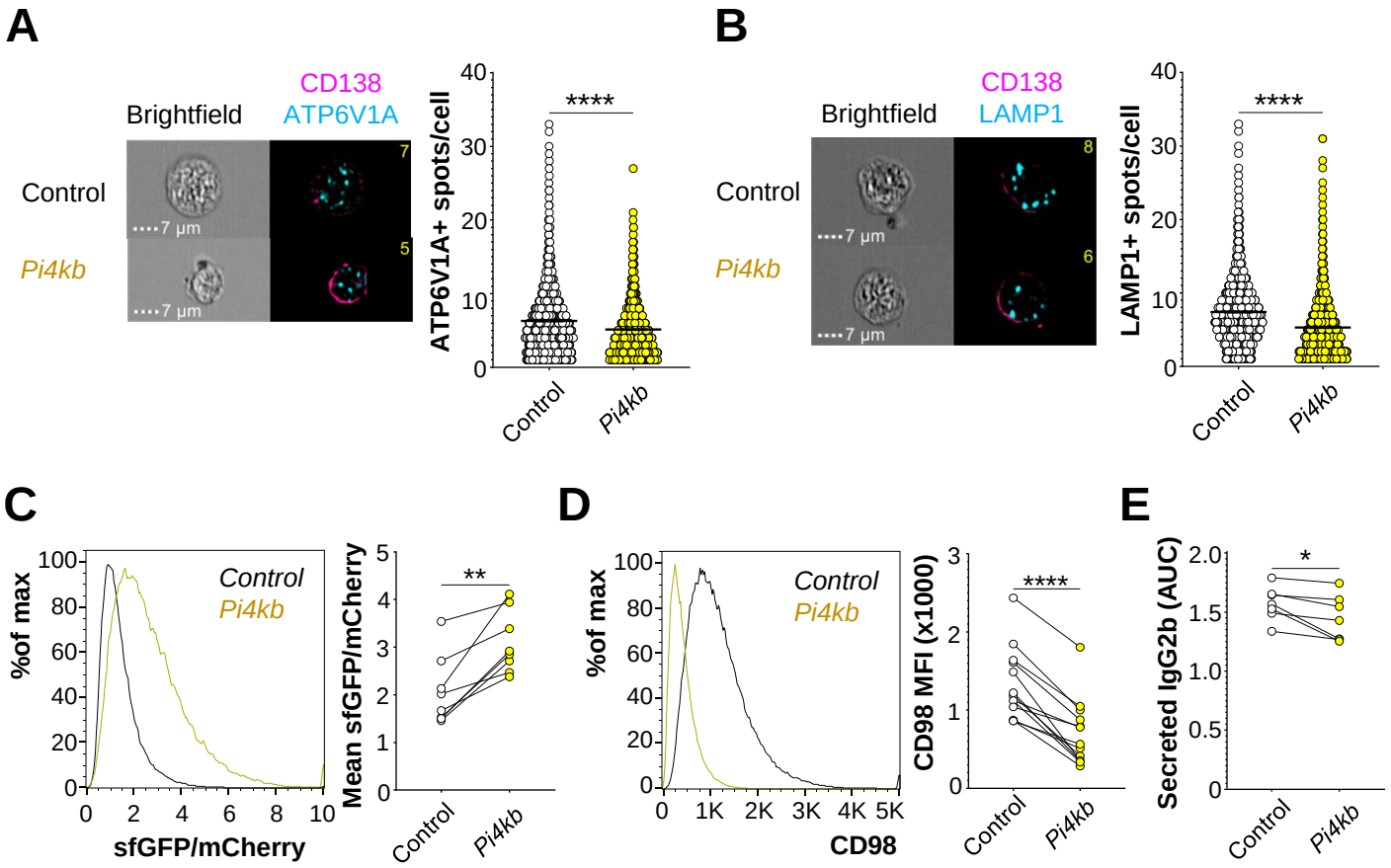
A
Brightfield
CD138
ATP6V1A
Control
Pi4kb
7 µm
7 µm
7
5
ATP6V1A+ spots/cell
****
Control
Pi4kb
B
Brightfield
CD138
LAMP1
Control
Pi4kb
7 µm
7 µm
8
6
LAMP1+ spots/cell
****
Control
Pi4kb
C
%of max
Control
Pi4kb
sfGFP/mCherry
Mean sfGFP/mCherry
**
Control
Pi4kb
D
%of max
Control
Pi4kb
CD98
CD98 MFI (x1000)
****
Control
Pi4kb
E
Secreted IgG2b (AUC)
*
Control
Pi4kb

717 **Figure 6: Ablation of *Pi4kb* reduces acidic vacuoles and antibody secretion**

718 **(A)** 5TGM1-Cas9 cells transduced with control gRNA (black) and *Pi4kb*-targeting gRNA
719 (yellow) and then scored for intracellular ATP6V1A+ spots/cell. Representative images
720 for each of the groups (left) and numbers of ATP6V1A+ spots/cell (right) were
721 quantified. Each circle represents one cell. Pooled data from 4236-4368 cells across 3
722 independent experiments. *p<0.05 by an unpaired t-test with Welch's correction.

723 **(B)** Groups in (A) were scored for intracellular LAMP1+ spots/cell. Representative
724 images for each of the groups (left) and numbers of LAMP1+ spots/cell (right) were
725 quantified. Each circle represents one cell. Pooled data from 4830-4837 cells across 3
726 independent experiments. *p<0.05 by an unpaired t-test with Welch's correction.

727 **(C)** 5TGM1-Cas9-pHLARE cells were transduced with lentivirus containing gRNA
728 targeting *Pi4kb* along with a control gRNA. Representative histogram (left) of the ratio of
729 sfGFP to mCherry MFI in control gRNA (black) and *Pi4kb*-targeting gRNA (yellow)
730 groups. Quantification of mean sfGFP/mCherry ratio (right) in control and knockout
731 cultures. Each circle represents values from a single group and groups within the same
732 experiment are joined by a line. Pooled data from 7 independent experiments. *p<0.05
733 by a paired t-test.

734 **(D)** Surface CD98 expression on groups in (C). Representative histogram (left) and
735 quantified CD98 MFI (right) are shown. Combined data from 13 experiments. *p<0.05 by
736 a paired t-test.

737 **(E)** Secreted IgG2b from culture supernatant of groups in (C) were quantified by ELISA.

738 AUC for each group is shown. Pooled data from 7 experiments. *$p<0.05$ by a paired t-

739 test.

740

Figure 7

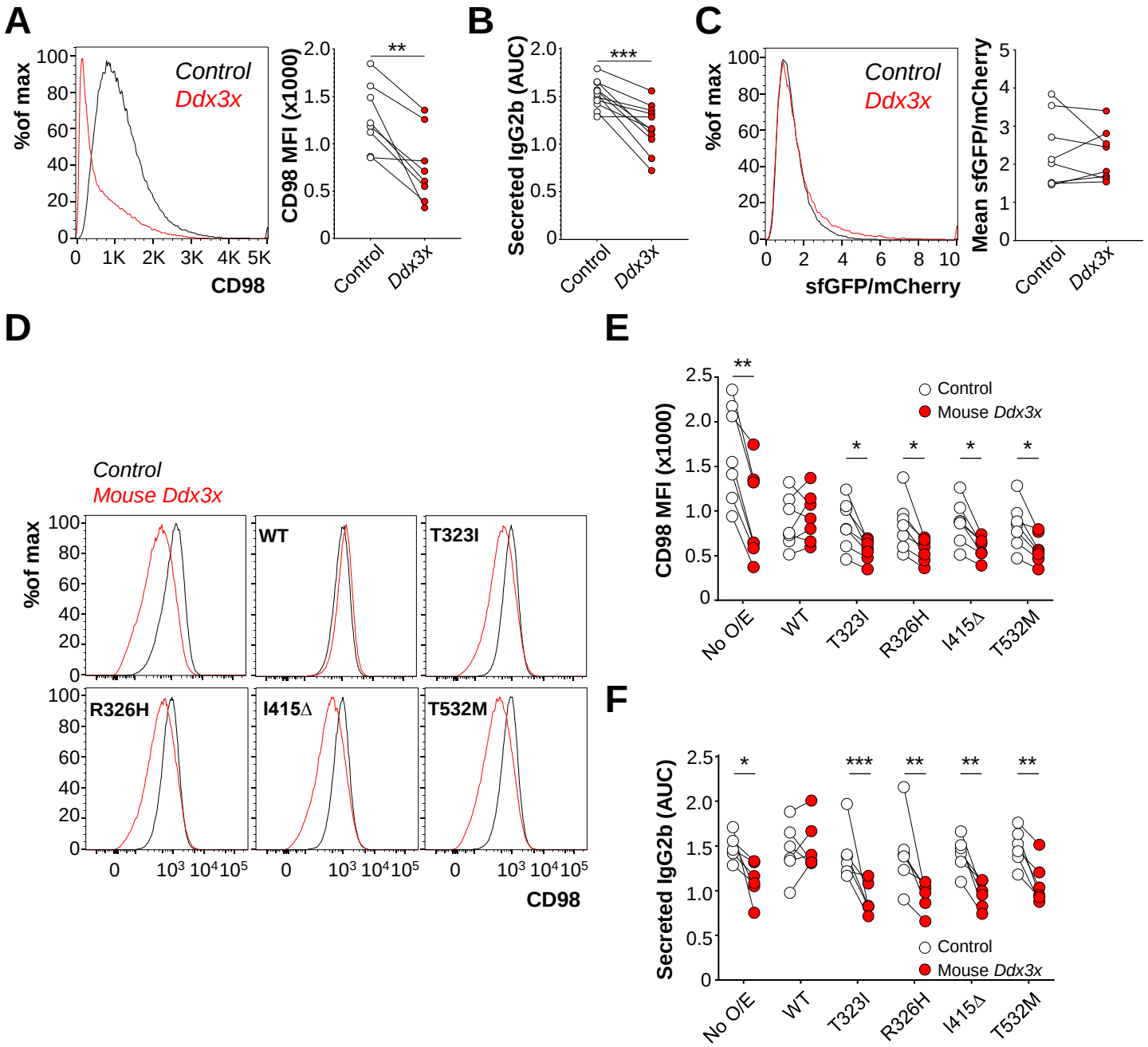
A
%of max
Control
Ddx3x
CD98
CD98 MFI (x1000)
**
Control
Ddx3x
B
Secreted IgG2b (AUC)
***
Control
Ddx3x
C
%of max
Control
Ddx3x
sfGFP/mCherry
Mean sfGFP/mCherry
Control
Ddx3x
D
Control
Mouse Ddx3x
%of max
WT
T323I
R326H
I415Δ
T532M
CD98
E
CD98 MFI (x1000)
Control
Mouse Ddx3x
No O/E
WT
T323I
R326H
I415Δ
T532M
F
Secreted IgG2b (AUC)
Control
Mouse Ddx3x
No O/E
WT
T323I
R326H
I415Δ
T532M

741 **Figure 7: DDX3X regulates antibody secretion independent of vacuolar**

742 **acidification**

743 **(A)** Surface CD98 expression on 5TGM1-Cas9 cells transduced with control gRNA or

744 gRNA targeting *Ddx3x*. Representative histogram (left) and quantified CD98 MFI (right)

745 are shown. Each circle represents values from cells in one well and are connected with

746 groups from the same experiment with a line. Combined data from 8 experiments.

747 *$p<0.05$ by a paired t-test.

748 **(B)** IgG2b antibody levels in culture supernatants of cells in (A). AUC for each group is

749 shown. Pooled data from 11 independent experiments. *$p<0.05$ by a paired t-test.

750 **(C)** 5TGM1-Cas9-pHLARE cells were transduced with lentivirus containing gRNA

751 targeting *Ddx3x* as well as a control gRNA. Representative histogram (left) of the ratio of

752 sfGFP to mCherry MFI in control gRNA (black) and *Ddx3x*-targeting gRNA (red) groups.

753 Quantification of mean sfGFP/mCherry ratio (right) in control and knockout cultures is

754 shown. Each circle represents a single group and groups within the same experiment

755 are joined by a line. Pooled data from 8 experiments. No significance observed by a

756 paired t-test.

757 **(D)** 5TGM1-Cas9 cells overexpressing hsDDX3X or catalytically inactive hsDDX3X

758 mutants were transduced with control gRNA or gRNA targeting mouse *Ddx3x*.

759 Representative histograms for surface CD98 distribution on cells transduced with

760 control gRNA (black) and mouse *Ddx3x* (red) are shown for cells without overexpression

761 (top left), cells overexpressing WT DDX3X (top center), and cells overexpressing
762 indicated mutant DDX3X (remaining squares).

763 **(E)** Quantification of surface CD98 expression on cells in (D) as well as cells
764 overexpressing DDX3X mutants. Each circle represents a single group and groups
765 within the same experiment are joined by a line. Pooled data from 6 independent
766 experiments. *$p<0.05$ by two-way ANOVA with Sidak's correction.

767 **(F)** Culture supernatants of all groups in (D) were assessed for secreted IgG2b by
768 ELISA. AUC for each group is shown. Pooled data from 6 experiments. *$p<0.05$ by two-
769 way ANOVA with Sidak's correction.

770

Figure 8

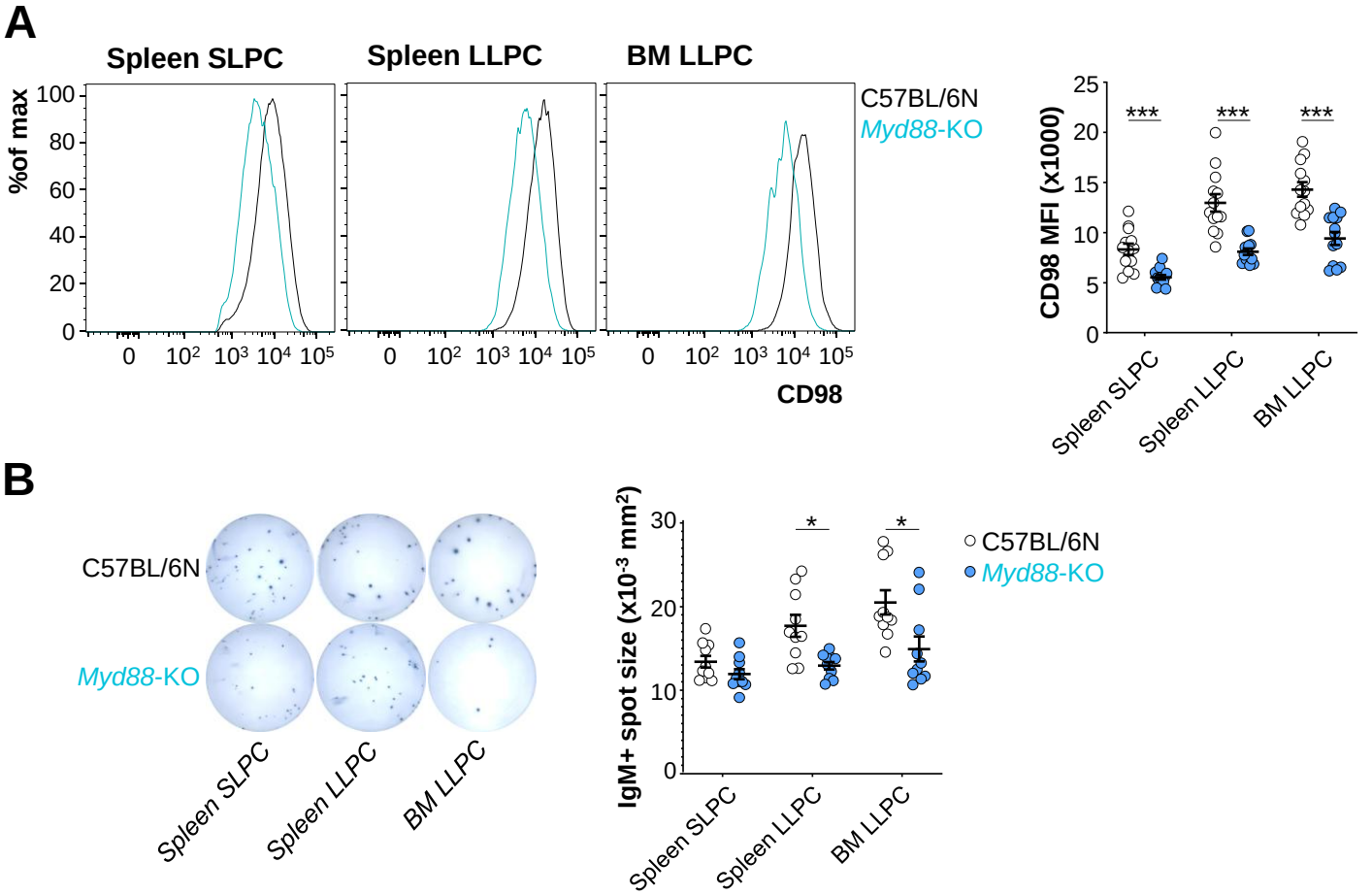
A
Spleen SLPC
Spleen LLPC
BM LLPC
%of max
C57BL/6N
Myd88-KO
CD98
CD98 MFI (x1000)
***
B
C57BL/6N
Myd88-KO
Spleen SLPC
Spleen LLPC
BM LLPC
IgM+ spot size (x10-3 mm2)
*

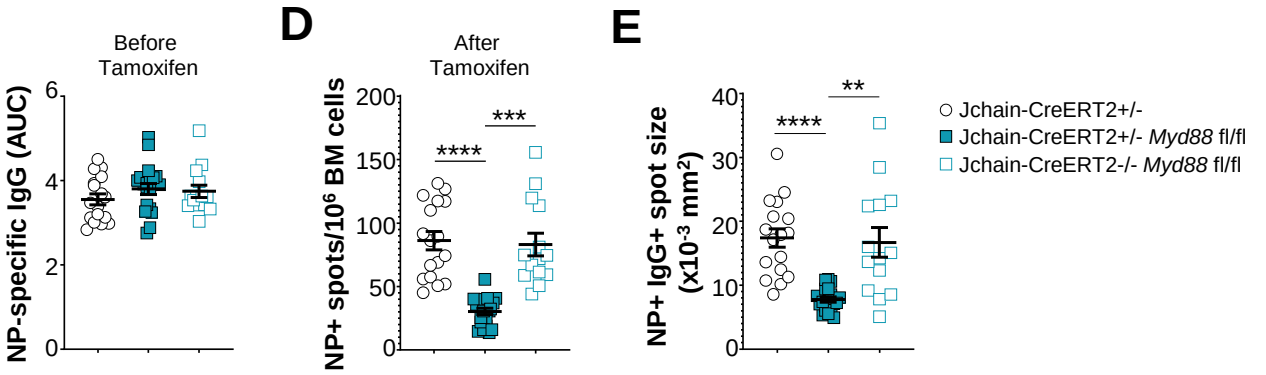
C
Before Tamoxifen
NP-specific IgG (AUC)
D
After Tamoxifen
NP+ spots/10^6 BM cells
****
***
E
NP+ IgG+ spot size (x10-3 mm2)
**
Jchain-CreERT2+/-
Jchain-CreERT2+/- Myd88 fl/fl
Jchain-CreERT2-/- Myd88 fl/fl

771 **Figure 8: Plasma cell intrinsic MYD88 promotes antibody secretory capacity and**
772 **longevity**

773 **(A)** Representative histograms of surface CD98 levels on IgM+ splenic SLPCs (left),
774 splenic LLPCs (center), and bone marrow LLPCs (right) from C57BL/6N (black) and
775 *Myd88*-KO mice (blue). CD98 MFI was then quantified on indicated groups. Each circle
776 is representative of a single mouse. Pooled data from 13 mice of each genotype across
777 4 independent experiments. *p<0.05 by two-way ANOVA with Sidak's correction.

778 **(B)** Indicated IgM+ plasma cell populations were purified from the spleens and bone
779 marrows of C57BL/6N (black) and *Myd88*-KO mice (blue) and seeded into an ELISpot
780 plate. Representative images showing spots from indicated plasma cell subset from
781 indicated mice are shown (left). Spot sizes of IgM-secreting plasma cells are quantified
782 (right), where each circle represents plasma cells from a single mouse. Combined data
783 from 10 mice across 3 experiments. *p<0.05 by two-way ANOVA with Sidak's
784 correction.

785 **(C)** Serum NP-specific IgG levels in Jchain-CreERT2+/- (black, filled circles), Jchain-
786 CreERT2+/- *Myd88* fl/fl (blue, filled squares), and Jchain-CreERT2-/- *Myd88* fl/fl (blue,
787 open squares) at 8 weeks post immunization with NP-CGG in Alhydrogel. Each square
788 represents a single mouse. Pooled data from 14-20 mice per group across 3 different
789 experiments. No statistical significance observed by repeated measures one-way
790 ANOVA with Dunnett's correction.

791 **(D)** Mice in (C) were placed on tamoxifen chow for 14 days. CD138+ bone marrow cells
792 were enriched and seeded into an ELISpot plate. Numbers of NP-specific IgG+ spots
793 per million cells are quantified for each mouse and represented. *$p<0.05$ by repeated
794 measures one-way ANOVA with Dunnett's correction.

795 **(E)** NP-specific IgG spot sizes in (D) were quantified and shown. *$p<0.05$ by repeated
796 measures one-way ANOVA with Dunnett's correction.

797

Figure 9

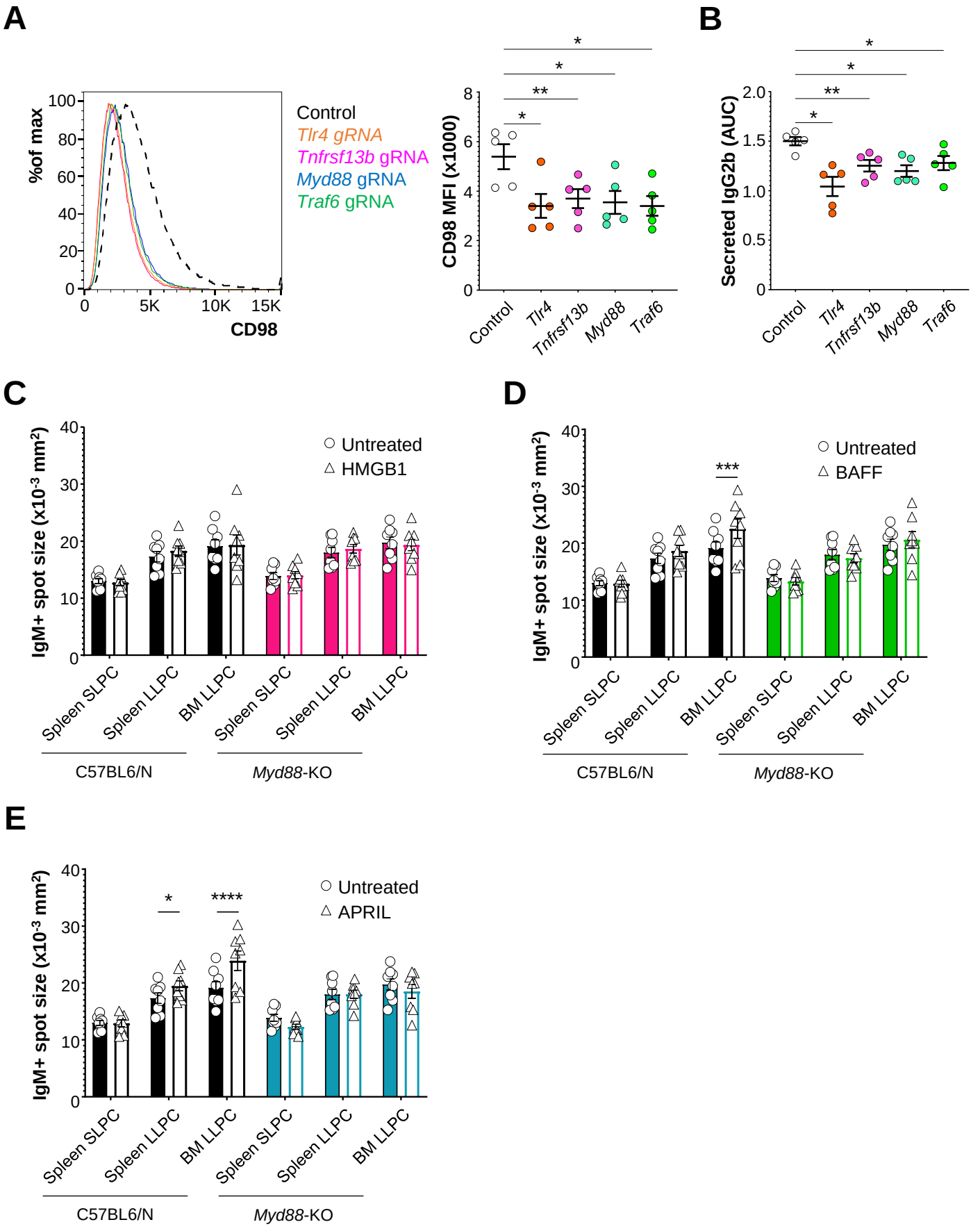
A
%of max
100
80
60
40
20
0
0
5K
10K
15K
CD98
Control
Tlr4 gRNA
Tnfrsf13b gRNA
Myd88 gRNA
Traf6 gRNA
CD98 MFI (x1000)
8
6
4
2
0
*
*
**
*
Control
Tlr4
Tnfrsf13b
Myd88
Traf6
B
Secreted IgG2b (AUC)
2.0
1.5
1.0
0.5
0
*
*
**
*
Control
Tlr4
Tnfrsf13b
Myd88
Traf6
C
IgM+ spot size (x10-3 mm2)
40
30
20
10
0
Untreated
HMGB1
Spleen SLPC
Spleen LLPC
BM LLPC
Spleen SLPC
Spleen LLPC
BM LLPC
C57BL6/N
Myd88-KO
D
IgM+ spot size (x10-3 mm2)
40
30
20
10
0
***
Untreated
BAFF
Spleen SLPC
Spleen LLPC
BM LLPC
Spleen SLPC
Spleen LLPC
BM LLPC
C57BL6/N
Myd88-KO
E
IgM+ spot size (x10-3 mm2)
40
30
20
10
0
*
****
Untreated
APRIL
Spleen SLPC
Spleen LLPC
BM LLPC
Spleen SLPC
Spleen LLPC
BM LLPC
C57BL6/N
Myd88-KO

798 **Figure 9: BAFF and APRIL promotes antibody secretory capacity in a MYD88-**
799 **dependent manner**

800 **(A)** 5TGM1-Cas9 cells were transduced with gRNA targeting *Tlr4*, *Tnfrsf13b*, *Myd88*, or
801 *Traf6*. Representative histograms (left) showing surface CD98 levels in transduced
802 groups (colored) relative to control gRNA transduced cells (black dashed). CD98 MFI
803 (right) was quantified across 5 independent experiments. Each circle represents values
804 from cells in a single well. *p<0.05 by repeated measures one-way ANOVA with
805 Dunnett's correction.

806 **(B)** Secreted IgG2b from culture supernatant of groups in (A) were quantified by ELISA.
807 AUC for each group is shown. Pooled data from 5 experiments. *p<0.05 by repeated
808 measures one-way ANOVA with Dunnett's correction.

809 **(C-E)** Sorted plasma cell subsets from C57BL/6 or *Myd88*-KO mice were seeded into an
810 ELISpot plate with media containing (C) 10μg/mL HMGB-1, (D) 10ng/mL BAFF, or (E)
811 10ng/mL APRIL. Cells treated with media are indicated with black bars, while treated
812 groups are colored. Individual circles and triangles represent the mean IgM+ spot size
813 from one mouse and matching groups are joined by a line. Pooled data from 8 mice
814 across 4 experiments. *p<0.05 by Two-way ANOVA.

815

Supplementary Figure 1

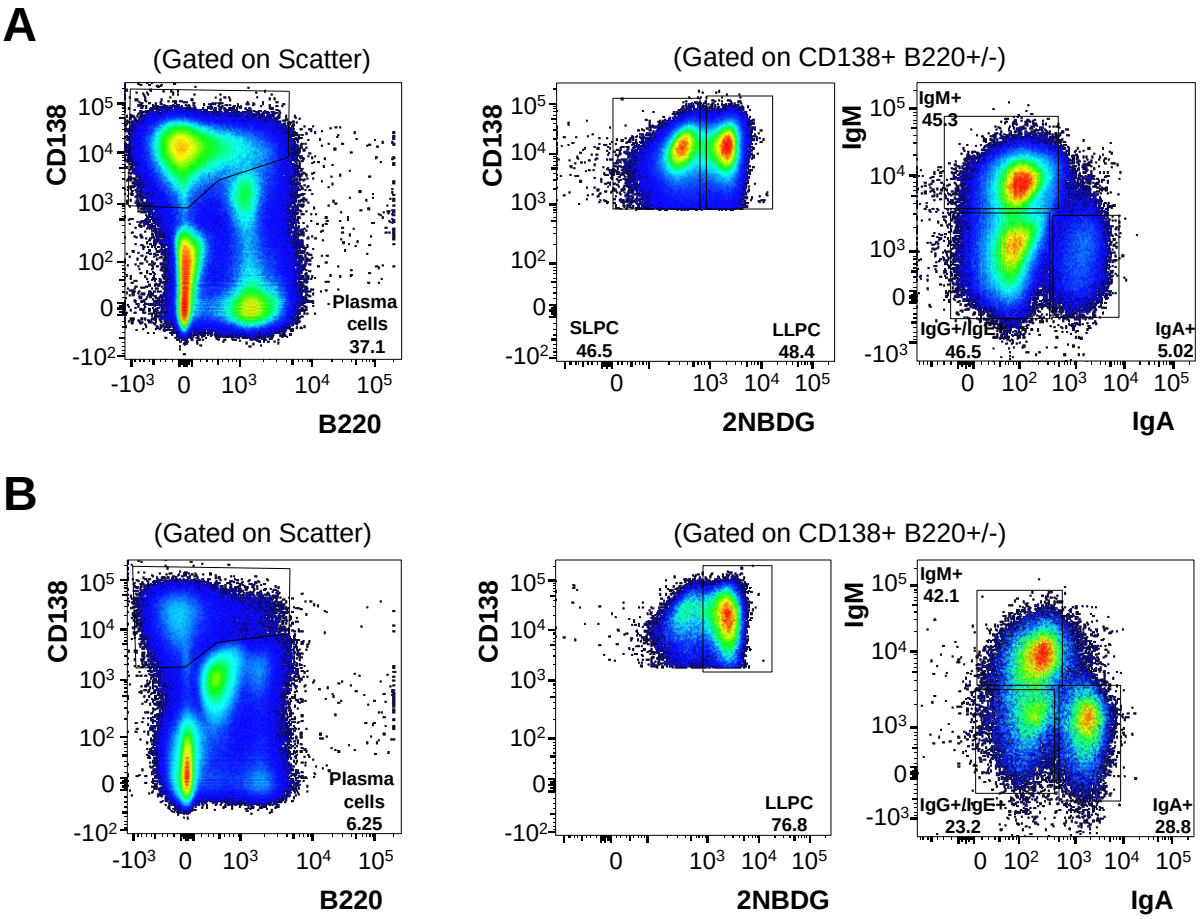

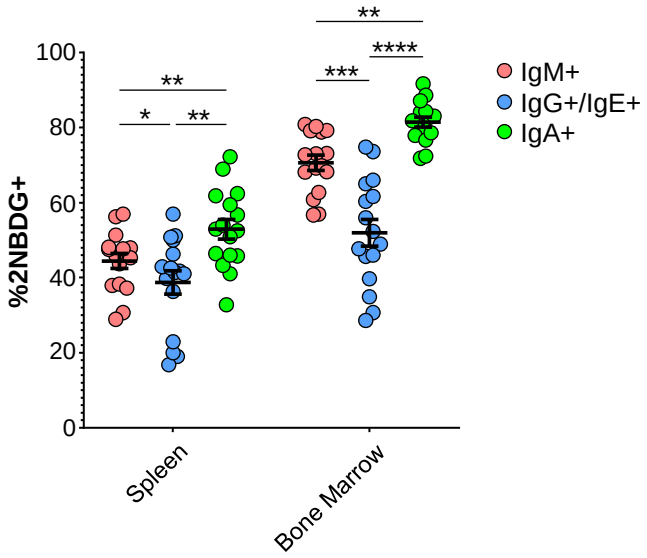

816 **Supplementary Figure 1: Murine plasma cell subsets have disparate proportions of**
817 **2NBDG+ cells.**

818 **(A)** Representative gating of mouse splenic plasma cells on enriched CD138+
819 splenocytes. Single cells were gated first as CD138+ B220+/- cells (left) and then
820 distinguished as 2NBDG- SLPC and 2NBDG+ LLPC (center), IgM+, IgA+, or IgG+ and
821 IgE+ (right).

822 **(B)** Representative gating of murine bone marrow plasma cell subsets gated as in (A).

823 **(C)** Long lived plasma cell frequencies as defined by 2NBDG uptake in mouse splenic
824 and bone marrow IgM+, IgG+ and IgE+, and IgA+ plasma cells. Each circle represents
825 values for the respective subset from one mouse. Pooled data from 16 mice across 4
826 experiments. *$p<0.05$ by two-way ANOVA with Tukey's correction.

827

Supplementary Figure 2

A

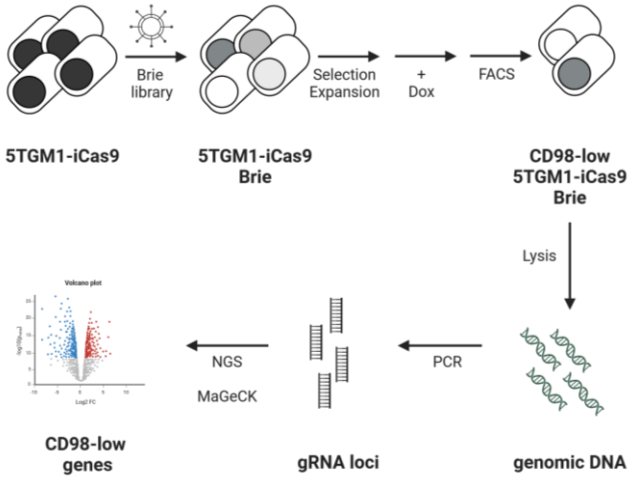

B

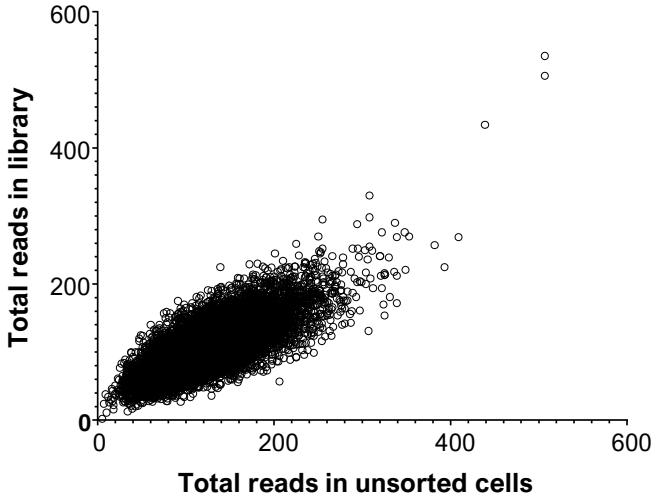

C

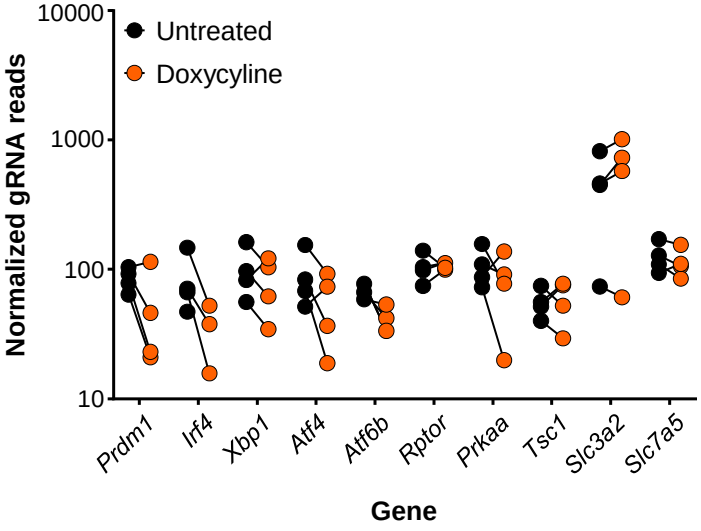

828 **Supplementary Figure 2: Cas9 induction leads to reduced abundance of gRNAs**

829 **targeting essential genes in 5TGM1-iCas9-Brie cultures**

830 **(A)** Schematic of genome-wide unbiased CRISPR-Cas9 screen in 5TGM1 cells.

831 **(B)** Scatter plot of gRNA read counts following next-generation sequencing of the

832 mouse Brie library (Y axis) against the corresponding read numbers in uninduced

833 5TGM1-iCas9-Brie cells (X axis). Each open circle represents one gRNA.

834 **(C)** 5TGM1-iCas9-Brie cells were left untreated or treated with Doxycycline. At day 7,

835 gRNA abundance was quantified from both groups using MaGeCK. Normalized counts

836 of gRNA targeting indicated genes are shown in both groups. Matching gRNAs are

837 connected by a line. Pooled data from 4 biological replicates.

838

Supplementary Figure 3

A

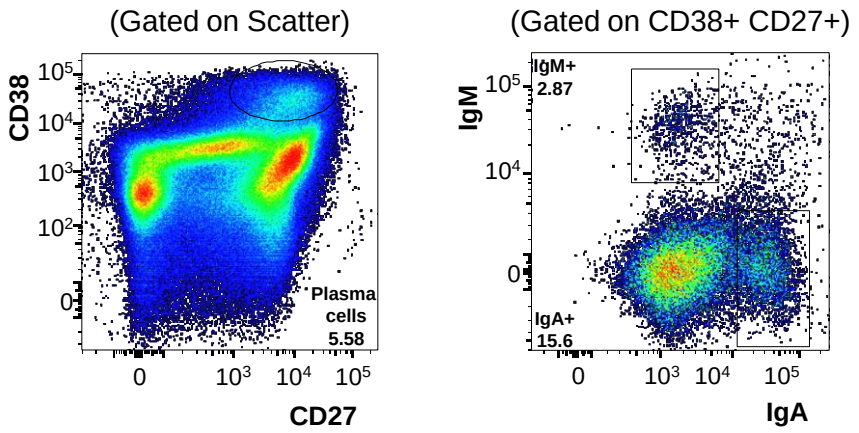

B

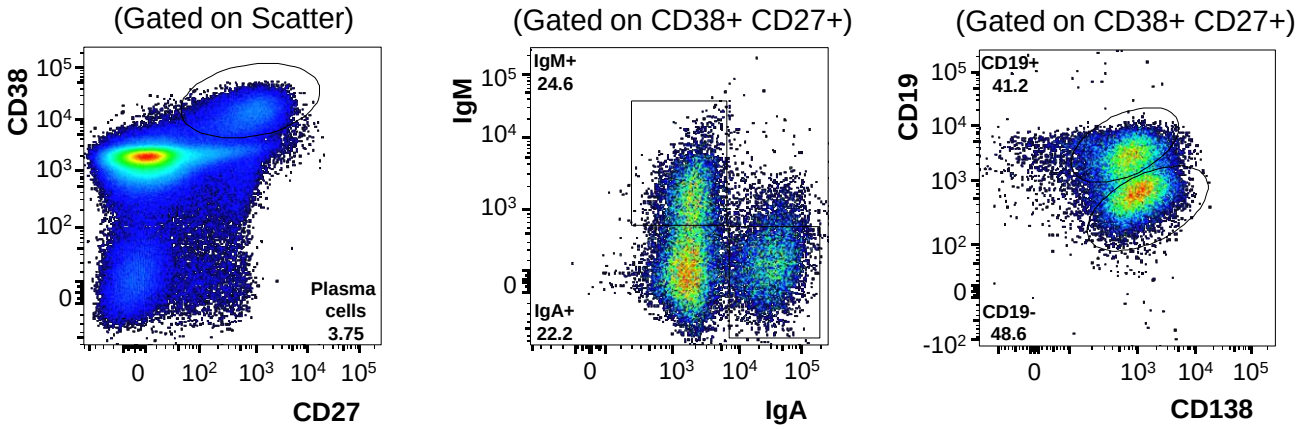

839 **Supplementary Figure 3: Identification of human plasma cell subsets**

840 **(A)** Representative gating of human tonsil plasma cells on CD38+ enriched cells. Cells
841 were identified as CD38+ CD27+ cells on single cells (left). Cells were then identified as
842 IgM- or IgA-secretors based surface expression of the respective isotype (right). Double
843 negative cells were presumed IgG+ and IgE+ plasma cells.

844 **(B)** Bone marrow plasma cells of various isotypes were gated like tonsillar plasma cells
845 as CD38+ CD27+ single cells (left, center). Human plasma cell subsets were then
846 identified as CD19+ or CD19- cells respectively (right).

847

Supplementary Figure 4

A

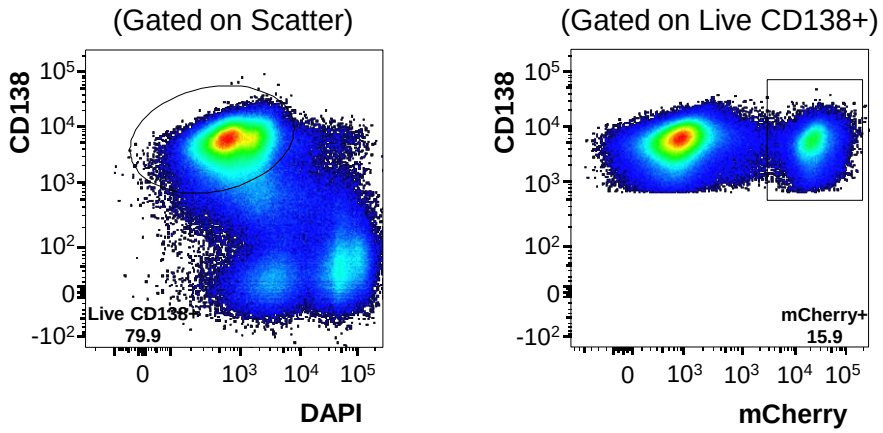

B

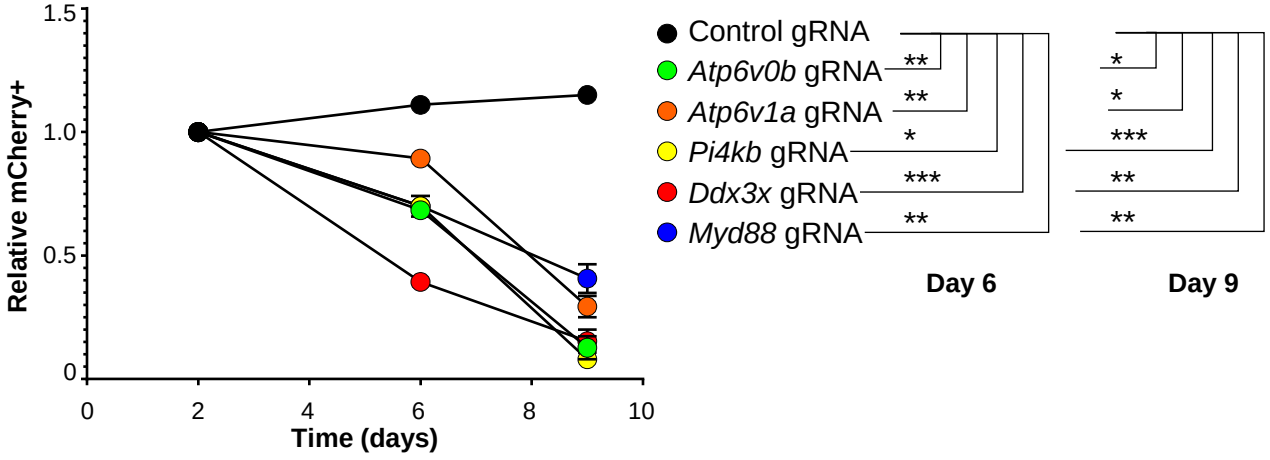

848 **Supplementary Figure 4: Perturbations in *Atp6v0b*, *Atp6v1a*, *Pi4kb*, *Ddx3x*, and**
849 ***Myd88* compromise cell survival**

850 **(A)** 5TGM1-Cas9 cells were transduced with lentivirus containing lentiGuide-mCherry
851 with control gRNA or gRNA targeting *Atp6v0b*, *Atp6v1a*, *Pi4kb*, *Ddx3x*, and *Myd88*.
852 Representative flow cytometry plots depicting live myeloma cells (left) at day 2 post
853 transduction with mCherry+ frequencies on them (right).

854 **(B)** Transduced cells in (A) were tracked in culture over time and mCherry+ frequencies
855 measured at days 2, 6, and 9 after transduction. mCherry+ frequencies were normalized
856 to frequencies at day 2. Each circle represents mCherry frequencies of cells in that well
857 and groups across time are linked by a line. Statistical significance for each group
858 relative to the control was calculated and indicated in the figure legend for day 6 and
859 day 9. *$p<0.05$ by two-way ANOVA.

860

861

Supplementary Figure 5

A

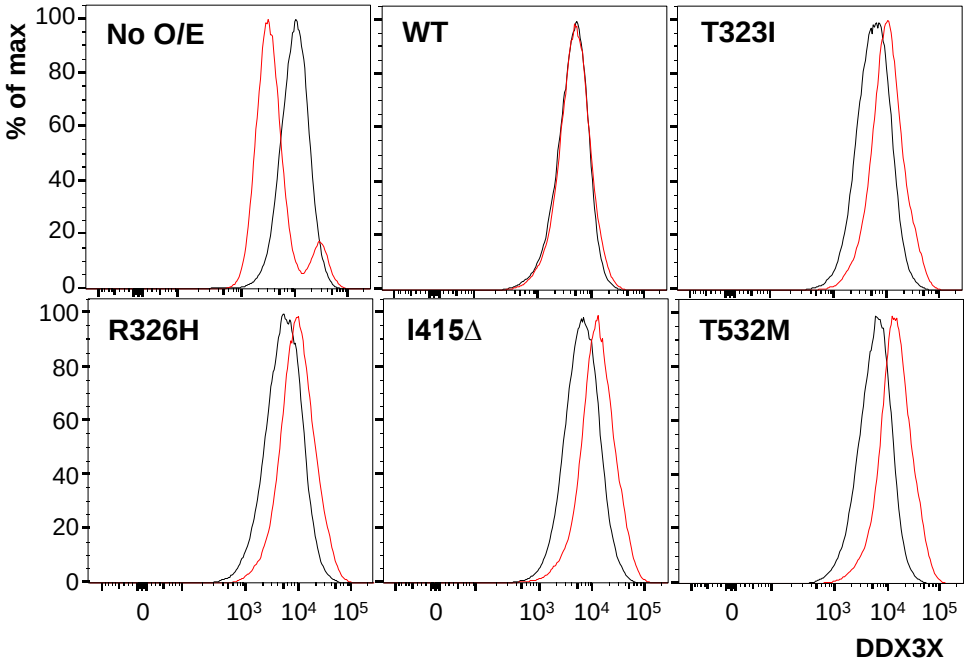

B

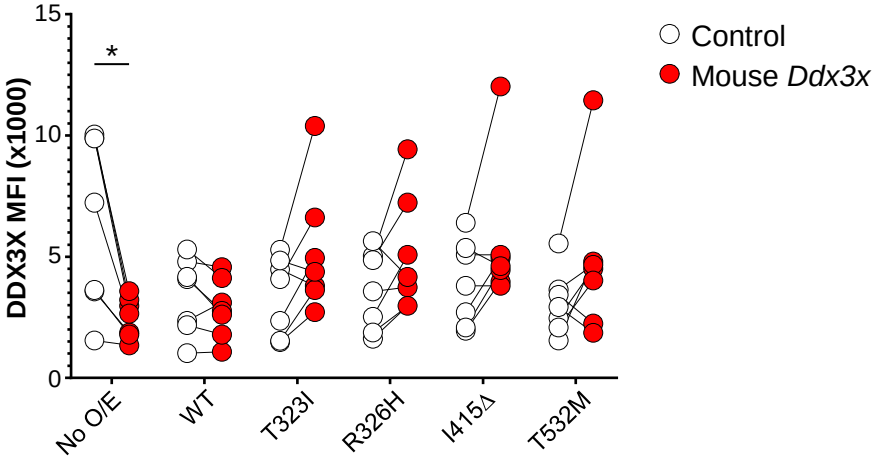

862 **Supplementary Figure 5: DDX3X protein levels are comparable in overexpression**
863 **cultures after ablation of endogenous mouse DDX3X.**

864 **(A)** 5TGM1-Cas9 cells overexpressing human DDX3X proteins were transduced with
865 gRNA targeting mouse *Ddx3x* (red) or control gRNA (black). Cells not overexpressing
866 DDX3X are shown on the top left. Representative histograms are shown for each of the
867 groups.

868 **(B)** Quantification of the MFI of various groups in (A) are displayed. Each line connects
869 groups within the same experiment. Pooled data from 7 independent experiments.
870 *$p<0.05$ by two-way ANOVA with Sidak's correction.

871

Supplementary Figure 6

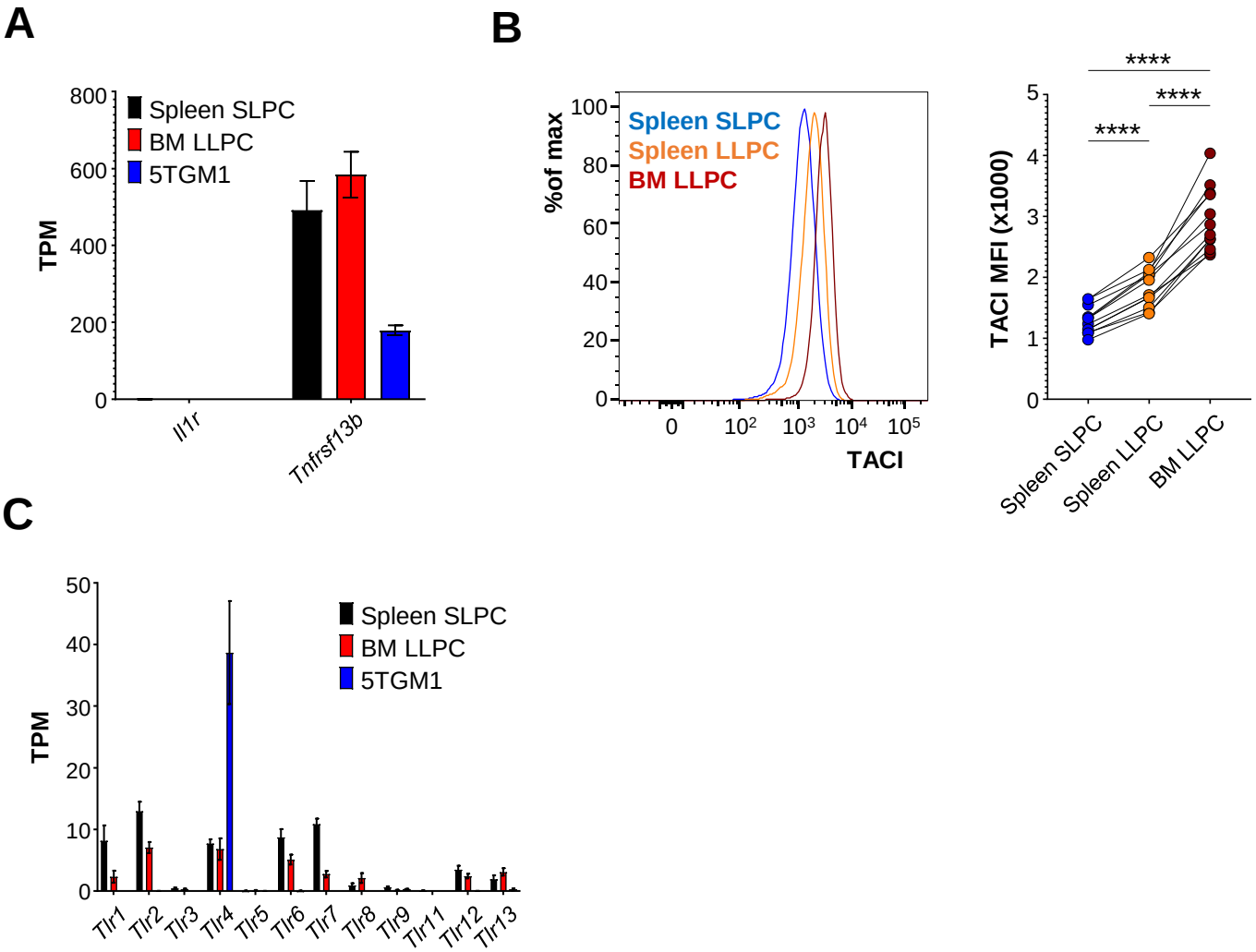

872 **Supplementary Figure 6: Plasma cell subsets express TACI and multiple TLRs but**
873 **not IL-1R.**

874 **(A)** TPM values of IL-1R (*Il1ra*) and TACI (*Tnfrsf13b*) showing data from splenic and
875 bone marrow plasma cell subsets from Lam WY *et al* (Cell Reports 2018) and 5TGM1
876 cells from D'Souza L *et al*, (PLoS One 2022). Pooled data from three independent
877 experiments.

878 **(B)** Representative histogram (left) showing surface expression of TACI on murine
879 plasma cell subsets as measured by flow cytometry. Each data point represents cells
880 from one mouse, and subsets from each mouse are connected by lines. Pooled data
881 from 12 mice across 7 experiments. *$p<0.05$ by paired one-way ANOVA with Tukey's
882 correction.

883 **(C)** TPM values of members of the TLR family of genes are shown for populations
884 mentioned in (A). Pooled data from three independent experiments.

885 **References**

886 Amanna, I.J., N.E. Carlson, and M.K. Slifka. 2007. Duration of humoral immunity to
887 common viral and vaccine antigens. *N Engl J Med*. 357:1903–1915.
888 doi:10.1056/NEJMoa066092.

889 Avery, D.T., S.L. Kalled, J.I. Ellyard, C. Ambrose, S.A. Bixler, M. Thien, R. Brink, F.
890 Mackay, P.D. Hodgkin, and S.G. Tangye. 2003. BAFF selectively enhances the
891 survival of plasmablasts generated from human memory B cells. *J Clin Invest*.
892 112:286–297. doi:10.1172/JCI18025.

893 Baba, T., and T. Balla. 2020. Emerging roles of phosphatidylinositol 4-phosphate and
894 phosphatidylinositol 4,5-bisphosphate as regulators of multiple steps in
895 autophagy. *J Biochem*. 168:329–336. doi:10.1093/jb/mvaa089.

896 Balla, A., G. Tuymetova, M. Barshishat, M. Geiszt, and T. Balla. 2002. Characterization of
897 type II phosphatidylinositol 4-kinase isoforms reveals association of the enzymes
898 with endosomal vesicular compartments. *J Biol Chem*. 277:20041–20050.
899 doi:10.1074/jbc.M111807200.

900 Belnoue, E., M. Pihlgren, T.L. McGaha, C. Tougne, A.-F. Rochat, C. Bossen, P.
901 Schneider, B. Huard, P.-H. Lambert, and C.-A. Siegrist. 2008. APRIL is critical for
902 plasmablast survival in the bone marrow and poorly expressed by early-life bone
903 marrow stromal cells. *Blood*. 111:2755–2764. doi:10.1182/blood-2007-09-
904 110858.

905 Benhamron, S., S.P. Pattanayak, M. Berger, and B. Tirosh. 2015. mTOR activation
906 promotes plasma cell differentiation and bypasses XBP-1 for immunoglobulin
907 secretion. *Mol Cell Biol*. 35:153–166. doi:10.1128/MCB.01187-14.

908 Benson, M.J., S.R. Dillon, E. Castigli, R.S. Geha, S. Xu, K.-P. Lam, and R.J. Noelle. 2008.
909 Cutting edge: the dependence of plasma cells and independence of memory B
910 cells on BAFF and APRIL. *J Immunol*. 180:3655–3659.
911 doi:10.4049/jimmunol.180.6.3655.

912 Bowman, E.J., A. Siebers, and K. Altendorf. 1988. Bafilomycins: a class of inhibitors of
913 membrane ATPases from microorganisms, animal cells, and plant cells. *Proc Natl*
914 *Acad Sci U S A*. 85:7972–7976. doi:10.1073/pnas.85.21.7972.

915 Brookens, S.K., S.H. Cho, P.J. Basso, and M.R. Boothby. 2020. AMPKα1 in B Cells
916 Dampens Primary Antibody Responses yet Promotes Mitochondrial Homeostasis
917 and Persistence of B Cell Memory. *J Immunol*. 205:3011–3022.
918 doi:10.4049/jimmunol.1901474.

919 Brynjolfsson, S.F., M. Mohaddes, J. Kärrholm, and M.-J. Wick. 2017. Long-lived plasma
920 cells in human bone marrow can be either CD19+ or CD19. *Blood Adv*. 1:835–
921 838. doi:10.1182/bloodadvances.2017004481.

922 Calviello, L., S. Venkataramanan, K.J. Rogowski, E. Wyler, K. Wilkins, M. Tejura, B. Thai,
923 J. Krol, W. Filipowicz, M. Landthaler, and S.N. Floor. 2021. DDX3 depletion
924 represses translation of mRNAs with complex 5' UTRs. *Nucleic Acids Res*.
925 49:5336–5350. doi:10.1093/nar/gkab287.

926 Cantor, J.M., and M.H. Ginsberg. 2012. CD98 at the crossroads of adaptive immunity
927 and cancer. *J Cell Sci*. 125:1373–1382. doi:10.1242/jcs.096040.

928 Casey, J.R., S. Grinstein, and J. Orlowski. 2010. Sensors and regulators of intracellular
929 pH. *Nat Rev Mol Cell Biol*. 11:50–61. doi:10.1038/nrm2820.

930 Cassese, G., S. Arce, A.E. Hauser, K. Lehnert, B. Moewes, M. Mostarac, G.
931 Muehlinghaus, M. Szyska, A. Radbruch, and R.A. Manz. 2003. Plasma cell
932 survival is mediated by synergistic effects of cytokines and adhesion-dependent
933 signals. *J Immunol*. 171:1684–1690. doi:10.4049/jimmunol.171.4.1684.

934 Collins, M.P., and M. Forgac. 2020. Regulation and function of V-ATPases in physiology
935 and disease. *Biochim Biophys Acta Biomembr*. 1862:183341.
936 doi:10.1016/j.bbamem.2020.183341.

937 Doench, J.G., N. Fusi, M. Sullender, M. Hegde, E.W. Vaimberg, K.F. Donovan, I. Smith, Z.
938 Tothova, C. Wilen, R. Orchard, H.W. Virgin, J. Listgarten, and D.E. Root. 2016.
939 Optimized sgRNA design to maximize activity and minimize off-target effects of
940 CRISPR-Cas9. *Nat Biotechnol*. 34:184–191. doi:10.1038/nbt.3437.

941 D'Souza, L., and D. Bhattacharya. 2019. Plasma cells: You are what you eat.
942 *Immunological Reviews*. 288:161–177. doi:10.1111/imr.12732.

943 D'Souza, L.J., S.H. Wright, and D. Bhattacharya. 2022. Genetic evidence that uptake of
944 the fluorescent analog 2NBDG occurs independently of known glucose
945 transporters. *PLoS One*. 17:e0261801. doi:10.1371/journal.pone.0261801.

946 Eslami, M., S. Schuepbach-Mallepell, D. Diana, L. Willen, C. Kowalczyk-Quintas, C.
947 Desponds, B. Peter, M. Vigolo, F. Renevey, O. Donzé, S.A. Luther, Ö. Yalkinoglu,
948 N. Alouche, and P. Schneider. 2024. Unique and redundant roles of mouse
949 BCMA, TACI, BAFF, APRIL, and IL-6 in supporting antibody-producing cells in
950 different tissues. *Proc Natl Acad Sci U S A*. 121:e2404309121.
951 doi:10.1073/pnas.2404309121.

952 Feral, C.C., N. Nishiya, C.A. Fenczik, H. Stuhlmann, M. Slepak, and M.H. Ginsberg. 2005.
953 CD98hc (SLC3A2) mediates integrin signaling. *Proc Natl Acad Sci U S A*.
954 102:355–360. doi:10.1073/pnas.0404852102.

955 Garrett, I.R., S. Dallas, J. Radl, and G.R. Mundy. 1997. A murine model of human
956 myeloma bone disease. *Bone*. 20:515–520. doi:10.1016/s8756-3282(97)00056-2.

957 Gavin, A.L., K. Hoebe, B. Duong, T. Ota, C. Martin, B. Beutler, and D. Nemazee. 2006.
958 Adjuvant-enhanced antibody responses in the absence of toll-like receptor
959 signaling. *Science*. 314:1936–1938. doi:10.1126/science.1135299.

960 Godi, A., P. Pertile, R. Meyers, P. Marra, G. Di Tullio, C. Iurisci, A. Luini, D. Corda, and
961 M.A. De Matteis. 1999. ARF mediates recruitment of PtdIns-4-OH kinase-beta and
962 stimulates synthesis of PtdIns(4,5)P2 on the Golgi complex. *Nat Cell Biol*. 1:280–
963 287. doi:10.1038/12993.

964 Halliley, J.L., C.M. Tipton, J. Liesveld, A.F. Rosenberg, J. Darce, I.V. Gregoretti, L.
965 Popova, D. Kaminiski, C.F. Fucile, I. Albizua, S. Kyu, K.-Y. Chiang, K.T. Bradley, R.
966 Burack, M. Slifka, E. Hammarlund, H. Wu, L. Zhao, E.E. Walsh, A.R. Falsey, T.D.
967 Randall, W.C. Cheung, I. Sanz, and F.E.-H. Lee. 2015. Long-Lived Plasma Cells
968 Are Contained within the CD19(-)CD38(hi)CD138(+) Subset in Human Bone
969 Marrow. *Immunity*. 43:132–145. doi:10.1016/j.immuni.2015.06.016.

970 He, B., R. Santamaria, W. Xu, M. Cols, K. Chen, I. Puga, M. Shan, H. Xiong, J.B. Bussel,
971 A. Chiu, A. Puel, J. Reichenbach, L. Marodi, R. Döffinger, J. Vasconcelos, A.
972 Issekutz, J. Krause, G. Davies, X. Li, B. Grimbacher, A. Plebani, E. Meffre, C.
973 Picard, C. Cunningham-Rundles, J.-L. Casanova, and A. Cerutti. 2010. The
974 transmembrane activator TACI triggers immunoglobulin class switching by
975 activating B cells through the adaptor MyD88. *Nat Immunol*. 11:836–845.
976 doi:10.1038/ni.1914.

977 Hou, B., B. Reizis, and A.L. DeFranco. 2008. Toll-like receptors activate innate and
978 adaptive immunity by using dendritic cell-intrinsic and -extrinsic mechanisms.
979 *Immunity*. 29:272–282. doi:10.1016/j.immuni.2008.05.016.

980 Hu, C.-C.A., S.K. Dougan, S.V. Winter, A.W. Paton, J.C. Paton, and H.L. Ploegh. 2009.
981 Subtilase cytotoxin cleaves newly synthesized BiP and blocks antibody secretion
982 in B lymphocytes. *J Exp Med*. 206:2429–2440. doi:10.1084/jem.20090782.

983 Ishikawa, M., Z.S. Hasanali, Y. Zhao, A. Das, M. Lavaert, C.J. Roman, J. Londregan, D.
984 Allman, and A. Bhandoola. 2024. Bone marrow plasma cells require P2RX4 to
985 sense extracellular ATP. *Nature*. 626:1102–1107. doi:10.1038/s41586-024-
986 07047-2.

987 Jones, D.D., B.T. Gaudette, J.R. Wilmore, I. Chernova, A. Bortnick, B.M. Weiss, and D.
988 Allman. 2016. mTOR has distinct functions in generating versus sustaining
989 humoral immunity. *J Clin Invest*. 126:4250–4261. doi:10.1172/JCI86504.

990 Lai, M.-C., Y.-H.W. Lee, and W.-Y. Tarn. 2008. The DEAD-box RNA helicase DDX3
991 associates with export messenger ribonucleoproteins as well as tip-associated

992 protein and participates in translational control. *Mol Biol Cell*. 19:3847–3858.
993 doi:10.1091/mbc.e07-12-1264.

994 Lam, T., D.V. Kulp, R. Wang, Z. Lou, J. Taylor, C.E. Rivera, H. Yan, Q. Zhang, Z. Wang, H.
995 Zan, D.N. Ivanov, G. Zhong, P. Casali, and Z. Xu. 2016. Small Molecule Inhibition
996 of Rab7 Impairs B Cell Class Switching and Plasma Cell Survival To Dampen the
997 Autoantibody Response in Murine Lupus. *J Immunol*. 197:3792–3805.
998 doi:10.4049/jimmunol.1601427.

999 Lam, W.Y., A. Jash, C.-H. Yao, L. D'Souza, R. Wong, R.M. Nunley, G.P. Meares, G.J.
1000 Patti, and D. Bhattacharya. 2018. Metabolic and Transcriptional Modules
1001 Independently Diversify Plasma Cell Lifespan and Function. *Cell Rep*. 24:2479-
1002 2492.e6. doi:10.1016/j.celrep.2018.07.084.

1003 Lennox, A.L., M.L. Hoye, R. Jiang, B.L. Johnson-Kerner, L.A. Suit, S. Venkataramanan,
1004 C.J. Sheehan, F.C. Alsina, B. Fregeau, K.A. Aldinger, C. Moey, I. Lobach, A.
1005 Afenjar, D. Babovic-Vuksanovic, S. Bézieau, P.R. Blackburn, J. Bunt, L. Burglen,
1006 P.M. Campeau, P. Charles, B.H.Y. Chung, B. Cogné, C. Curry, M.D. D'Agostino,
1007 N. Di Donato, L. Faivre, D. Héron, A.M. Innes, B. Isidor, B. Keren, A. Kimball, E.W.
1008 Klee, P. Kuentz, S. Küry, D. Martin-Coignard, G. Mirzaa, C. Mignot, N. Miyake, N.
1009 Matsumoto, A. Fujita, C. Nava, M. Nizon, D. Rodriguez, L.S. Blok, C. Thauvin-
1010 Robinet, J. Thevenon, M. Vincent, A. Ziegler, W. Dobyns, L.J. Richards, A.J.
1011 Barkovich, S.N. Floor, D.L. Silver, and E.H. Sherr. 2020. Pathogenic DDX3X
1012 Mutations Impair RNA Metabolism and Neurogenesis during Fetal Cortical
1013 Development. *Neuron*. 106:404-420.e8. doi:10.1016/j.neuron.2020.01.042.

1014 Li, W., H. Xu, T. Xiao, L. Cong, M.I. Love, F. Zhang, R.A. Irizarry, J.S. Liu, M. Brown, and
1015 X.S. Liu. 2014. MAGeCK enables robust identification of essential genes from
1016 genome-scale CRISPR/Cas9 knockout screens. *Genome Biol*. 15:554.
1017 doi:10.1186/s13059-014-0554-4.

1018 Liu, K., J. Tuazon, E.P. Karmele, D. Krishnamurthy, T. Perlor, M. Foong-Sobis, R.A.
1019 Karns, M. Mandal, D. Reynaud, R.H. Scofield, J.M. Penninger, J.B. Harley, and
1020 S.N. Waggoner. 2018. *Ddx3x* regulates B-cell development and light chain
1021 recombination in mice. doi:10.1101/452086.

1022 Martincic, K., S.A. Alkan, A. Cheatle, L. Borghesi, and C. Milcarek. 2009. Transcription
1023 elongation factor ELL2 directs immunoglobulin secretion in plasma cells by
1024 stimulating altered RNA processing. *Nat Immunol*. 10:1102–1109.
1025 doi:10.1038/ni.1786.

1026 Mei, H.E., I. Wirries, D. Frölich, M. Brisslert, C. Giesecke, J.R. Grün, T. Alexander, S.
1027 Schmidt, K. Luda, A.A. Kühl, R. Engelmann, M. Dürr, T. Scheel, M. Bokarewa, C.
1028 Perka, A. Radbruch, and T. Dörner. 2015. A unique population of IgG-expressing

1029 plasma cells lacking CD19 is enriched in human bone marrow. *Blood*. 125:1739–
1030 1748. doi:10.1182/blood-2014-02-555169.

1031 Meyers, R., and L.C. Cantley. 1997. Cloning and characterization of a wortmannin-
1032 sensitive human phosphatidylinositol 4-kinase. *J Biol Chem*. 272:4384–4390.
1033 doi:10.1074/jbc.272.7.4384.

1034 Minnich, M., H. Tagoh, P. Bönelt, E. Axelsson, M. Fischer, B. Cebolla, A. Tarakhovsky,
1035 S.L. Nutt, M. Jaritz, and M. Busslinger. 2016. Multifunctional role of the
1036 transcription factor Blimp-1 in coordinating plasma cell differentiation. *Nat*
1037 *Immunol*. 17:331–343. doi:10.1038/ni.3349.

1038 Ng, P.K.-S., J. Li, K.J. Jeong, S. Shao, H. Chen, Y.H. Tsang, S. Sengupta, Z. Wang, V.H.
1039 Bhavana, R. Tran, S. Soewito, D.C. Minussi, D. Moreno, K. Kong, T. Dogruluk, H.
1040 Lu, J. Gao, C. Tokheim, D.C. Zhou, A.M. Johnson, J. Zeng, C.K.M. Ip, Z. Ju, M.
1041 Wester, S. Yu, Y. Li, C.P. Vellano, N. Schultz, R. Karchin, L. Ding, Y. Lu, L.W.T.
1042 Cheung, K. Chen, K.R. Shaw, F. Meric-Bernstam, K.L. Scott, S. Yi, N. Sahni, H.
1043 Liang, and G.B. Mills. 2018. Systematic Functional Annotation of Somatic
1044 Mutations in Cancer. *Cancer Cell*. 33:450-462.e10.
1045 doi:10.1016/j.ccell.2018.01.021.

1046 Nguyen, D.C., S. Garimalla, H. Xiao, S. Kyu, I. Albizua, J. Galipeau, K.-Y. Chiang, E.K.
1047 Waller, R. Wu, G. Gibson, J. Roberson, F.E. Lund, T.D. Randall, I. Sanz, and F.E.-
1048 H. Lee. 2018. Factors of the bone marrow microniche that support human plasma
1049 cell survival and immunoglobulin secretion. *Nat Commun*. 9:3698.
1050 doi:10.1038/s41467-018-05853-7.

1051 Nguyen, D.C., I.T. Hentenaar, A. Morrison-Porter, D. Solano, N.S. Haddad, C. Castrillon,
1052 M.C. Runnstrom, P.A. Lamothe, J. Andrews, D. Roberts, S. Lonial, I. Sanz, and
1053 F.E.-H. Lee. 2024. SARS-CoV-2-specific plasma cells are not durably established
1054 in the bone marrow long-lived compartment after mRNA vaccination. *Nat Med*.
1055 doi:10.1038/s41591-024-03278-y.

1056 O'Connor, B.P., V.S. Raman, L.D. Erickson, W.J. Cook, L.K. Weaver, C. Ahonen, L.-L.
1057 Lin, G.T. Mantchev, R.J. Bram, and R.J. Noelle. 2004. BCMA is essential for the
1058 survival of long-lived bone marrow plasma cells. *J Exp Med*. 199:91–98.
1059 doi:10.1084/jem.20031330.

1060 Olotu, A., G. Fegan, J. Wambua, G. Nyangweso, K.O. Awuondo, A. Leach, M. Lievens, D.
1061 Leboulleux, P. Njuguna, N. Peshu, K. Marsh, and P. Bejon. 2013. Four-year
1062 efficacy of RTS,S/AS01E and its interaction with malaria exposure. *N Engl J Med*.
1063 368:1111–1120. doi:10.1056/NEJMoa1207564.

1064 Olsson, S.-E., L.L. Villa, R.L.R. Costa, C.A. Petta, R.P. Andrade, C. Malm, O.-E. Iversen, J.
1065 Høye, M. Steinwall, G. Riis-Johannessen, A. Andersson-Ellstrom, K. Elfgren, G.
1066 von Krogh, M. Lehtinen, J. Paavonen, G.M. Tamms, K. Giacoletti, L. Lupinacci,

1067 M.T. Esser, S.C. Vuocolo, A.J. Saah, and E. Barr. 2007. Induction of immune
1068 memory following administration of a prophylactic quadrivalent human
1069 papillomavirus (HPV) types 6/11/16/18 L1 virus-like particle (VLP) vaccine.
1070 *Vaccine*. 25:4931–4939. doi:10.1016/j.vaccine.2007.03.049.

1071 Parsa, R., H. Lund, A.-M. Georgoudaki, X.-M. Zhang, A. Ortlieb Guerreiro-Cacais, D.
1072 Grommisch, A. Warnecke, A.L. Croxford, M. Jagodic, B. Becher, M.C.I. Karlsson,
1073 and R.A. Harris. 2016. BAFF-secreting neutrophils drive plasma cell responses
1074 during emergency granulopoiesis. *J Exp Med*. 213:1537–1553.
1075 doi:10.1084/jem.20150577.

1076 Pasare, C., and R. Medzhitov. 2005. Control of B-cell responses by Toll-like receptors.
1077 *Nature*. 438:364–368. doi:10.1038/nature04267.

1078 Pédelacq, J.-D., S. Cabantous, T. Tran, T.C. Terwilliger, and G.S. Waldo. 2006.
1079 Engineering and characterization of a superfolder green fluorescent protein. *Nat*
1080 *Biotechnol*. 24:79–88. doi:10.1038/nbt1172.

1081 Pinter, T., M. Fischer, M. Schäfer, M. Fellner, J. Jude, J. Zuber, M. Busslinger, and M.
1082 Wöhner. 2022. Comprehensive CRISPR-Cas9 screen identifies factors which are
1083 important for plasmablast development. *Front Immunol*. 13:979606.
1084 doi:10.3389/fimmu.2022.979606.

1085 Pone, E.J., T. Lam, Z. Lou, R. Wang, Y. Chen, D. Liu, A.L. Edinger, Z. Xu, and P. Casali.
1086 2015. B cell Rab7 mediates induction of activation-induced cytidine deaminase
1087 expression and class-switching in T-dependent and T-independent antibody
1088 responses. *J Immunol*. 194:3065–3078. doi:10.4049/jimmunol.1401896.

1089 Purtha, W.E., T.F. Tedder, S. Johnson, D. Bhattacharya, and M.S. Diamond. 2011.
1090 Memory B cells, but not long-lived plasma cells, possess antigen specificities for
1091 viral escape mutants. *J Exp Med*. 208:2599–2606. doi:10.1084/jem.20110740.

1092 Reimold, A.M., N.N. Iwakoshi, J. Manis, P. Vallabhajosyula, E. Szomolanyi-Tsuda, E.M.
1093 Gravallese, D. Friend, M.J. Grusby, F. Alt, and L.H. Glimcher. 2001. Plasma cell
1094 differentiation requires the transcription factor XBP-1. *Nature*. 412:300–307.
1095 doi:10.1038/35085509.

1096 Robinson, M.J., Z. Ding, M.R. Dowling, D.L. Hill, R.H. Webster, C. McKenzie, C. Pitt, K.
1097 O'Donnell, J. Mulder, E. Brodie, P.D. Hodgkin, N.C. Wong, I. Quast, and D.M.
1098 Tarlinton. 2023. Intrinsically determined turnover underlies broad heterogeneity
1099 in plasma-cell lifespan. *Immunity*. 56:1596-1612.e4.
1100 doi:10.1016/j.immuni.2023.04.015.

1101 Rozanski, C.H., R. Arens, L.M. Carlson, J. Nair, L.H. Boise, A.A. Chanan-Khan, S.P.
1102 Schoenberger, and K.P. Lee. 2011. Sustained antibody responses depend on

1103 CD28 function in bone marrow-resident plasma cells. *J Exp Med*. 208:1435–1446.
1104 doi:10.1084/jem.20110040.

1105 Sanjana, N.E., O. Shalem, and F. Zhang. 2014. Improved vectors and genome-wide
1106 libraries for CRISPR screening. *Nat Methods*. 11:783–784.
1107 doi:10.1038/nmeth.3047.

1108 Sanson, K.R., R.E. Hanna, M. Hegde, K.F. Donovan, C. Strand, M.E. Sullender, E.W.
1109 Vaimberg, A. Goodale, D.E. Root, F. Piccioni, and J.G. Doench. 2018. Optimized
1110 libraries for CRISPR-Cas9 genetic screens with multiple modalities. *Nat Commun*.
1111 9:5416. doi:10.1038/s41467-018-07901-8.

1112 Sekiguchi, T., H. Iida, J. Fukumura, and T. Nishimoto. 2004. Human DDX3Y, the Y-
1113 encoded isoform of RNA helicase DDX3, rescues a hamster temperature-
1114 sensitive ET24 mutant cell line with a DDX3X mutation. *Exp Cell Res*. 300:213–
1115 222. doi:10.1016/j.yexcr.2004.07.005.

1116 Shaffer, A.L., M. Shapiro-Shelef, N.N. Iwakoshi, A.-H. Lee, S.-B. Qian, H. Zhao, X. Yu, L.
1117 Yang, B.K. Tan, A. Rosenwald, E.M. Hurt, E. Petroulakis, N. Sonenberg, J.W.
1118 Yewdell, K. Calame, L.H. Glimcher, and L.M. Staudt. 2004. XBP1, downstream of
1119 Blimp-1, expands the secretory apparatus and other organelles, and increases
1120 protein synthesis in plasma cell differentiation. *Immunity*. 21:81–93.
1121 doi:10.1016/j.immuni.2004.06.010.

1122 Shi, W., Y. Liao, S.N. Willis, N. Taubenheim, M. Inouye, D.M. Tarlinton, G.K. Smyth, P.D.
1123 Hodgkin, S.L. Nutt, and L.M. Corcoran. 2015. Transcriptional profiling of mouse B
1124 cell terminal differentiation defines a signature for antibody-secreting plasma
1125 cells. *Nat Immunol*. 16:663–673. doi:10.1038/ni.3154.

1126 Shih, J.-W., T.-Y. Tsai, C.-H. Chao, and Y.-H. Wu Lee. 2008. Candidate tumor
1127 suppressor DDX3 RNA helicase specifically represses cap-dependent translation
1128 by acting as an eIF4E inhibitory protein. *Oncogene*. 27:700–714.
1129 doi:10.1038/sj.onc.1210687.

1130 Smulski, C.R., and H. Eibel. 2018. BAFF and BAFF-Receptor in B Cell Selection and
1131 Survival. *Front Immunol*. 9:2285. doi:10.3389/fimmu.2018.02285.

1132 Soto-Rifo, R., P.S. Rubilar, T. Limousin, S. de Breyne, D. Décimo, and T. Ohlmann. 2012.
1133 DEAD-box protein DDX3 associates with eIF4F to promote translation of selected
1134 mRNAs. *EMBO J*. 31:3745–3756. doi:10.1038/emboj.2012.220.

1135 Sridhar, S., B. Patel, D. Aphkhazava, F. Macian, L. Santambrogio, D. Shields, and A.M.
1136 Cuervo. 2013. The lipid kinase PI4KIIIβ preserves lysosomal identity. *EMBO J*.
1137 32:324–339. doi:10.1038/emboj.2012.341.

1138 Szappanos, D., R. Tschismarov, T. Perlot, S. Westermayer, K. Fischer, E. Platanitis, F.
1139 Kallinger, M. Novatchkova, C. Lassnig, M. Müller, V. Sexl, K.L. Bennett, M. Foong-
1140 Sobis, J.M. Penninger, and T. Decker. 2018. The RNA helicase DDX3X is an
1141 essential mediator of innate antimicrobial immunity. *PLoS Pathog*. 14:e1007397.
1142 doi:10.1371/journal.ppat.1007397.

1143 Takeda, K., and S. Akira. 2004. TLR signaling pathways. *Semin Immunol*. 16:3–9.
1144 doi:10.1016/j.smim.2003.10.003.

1145 Taubenheim, N., D.M. Tarlinton, S. Crawford, L.M. Corcoran, P.D. Hodgkin, and S.L.
1146 Nutt. 2012. High rate of antibody secretion is not integral to plasma cell
1147 differentiation as revealed by XBP-1 deficiency. *J Immunol*. 189:3328–3338.
1148 doi:10.4049/jimmunol.1201042.

1149 Tellier, J., W. Shi, M. Minnich, Y. Liao, S. Crawford, G.K. Smyth, A. Kallies, M. Busslinger,
1150 and S.L. Nutt. 2016. Blimp-1 controls plasma cell function through the regulation
1151 of immunoglobulin secretion and the unfolded protein response. *Nat Immunol*.
1152 17:323–330. doi:10.1038/ni.3348.

1153 Trezise, S., I.Y. Kong, E.D. Hawkins, M.J. Herold, S.N. Willis, and S.L. Nutt. 2023. An
1154 arrayed CRISPR screen of primary B cells reveals the essential elements of the
1155 antibody secretion pathway. *Front Immunol*. 14:1089243.
1156 doi:10.3389/fimmu.2023.1089243.

1157 Webb, B.A., F.M. Aloisio, R.A. Charafeddine, J. Cook, T. Wittmann, and D.L. Barber.
1158 2021. pHLARE: a new biosensor reveals decreased lysosome pH in cancer cells.
1159 *Mol Biol Cell*. 32:131–142. doi:10.1091/mbc.E20-06-0383.

1160 White, M.T., R. Verity, J.T. Griffin, K.P. Asante, S. Owusu-Agyei, B. Greenwood, C.
1161 Drakeley, S. Gesase, J. Lusingu, D. Ansong, S. Adjei, T. Agbenyega, B. Ogutu, L.
1162 Otieno, W. Otieno, S.T. Agnandji, B. Lell, P. Kremsner, I. Hoffman, F. Martinson, P.
1163 Kamthunzu, H. Tinto, I. Valea, H. Sorgho, M. Oneko, K. Otieno, M.J. Hamel, N.
1164 Salim, A. Mtoro, S. Abdulla, P. Aide, J. Sacarlal, J.J. Aponte, P. Njuguna, K.
1165 Marsh, P. Bejon, E.M. Riley, and A.C. Ghani. 2015. Immunogenicity of the
1166 RTS,S/AS01 malaria vaccine and implications for duration of vaccine efficacy:
1167 secondary analysis of data from a phase 3 randomised controlled trial. *Lancet*
1168 *Infect Dis*. 15:1450–1458. doi:10.1016/S1473-3099(15)00239-X.

1169 Wilmore, J.R., B.T. Gaudette, D. Gomez Atria, T. Hashemi, D.D. Jones, C.A. Gardner,
1170 S.D. Cole, A.M. Misic, D.P. Beiting, and D. Allman. 2018. Commensal Microbes
1171 Induce Serum IgA Responses that Protect against Polymicrobial Sepsis. *Cell Host*
1172 *Microbe*. 23:302-311.e3. doi:10.1016/j.chom.2018.01.005.

1173 Wong, R., J.A. Belk, J. Govero, J.L. Uhrlaub, D. Reinartz, H. Zhao, J.M. Errico, L.
1174 D'Souza, T.J. Ripperger, J. Nikolich-Zugich, M.J. Shlomchik, A.T. Satpathy, D.H.
1175 Fremont, M.S. Diamond, and D. Bhattacharya. 2020. Affinity-Restricted Memory B

1176 Cells Dominate Recall Responses to Heterologous Flaviviruses. *Immunity*.
1177 53:1078-1094.e7. doi:10.1016/j.immuni.2020.09.001.

1178 Xiong, E., O. Popp, C. Salomon, P. Mertins, C. Kocks, K. Rajewsky, and V.T. Chu. 2022.
1179 A CRISPR/Cas9-mediated screen identifies determinants of early plasma cell
1180 differentiation. *Front Immunol*. 13:1083119. doi:10.3389/fimmu.2022.1083119.

1181 Yanagida, O., Y. Kanai, A. Chairoungdua, D.K. Kim, H. Segawa, T. Nii, S.H. Cha, H.
1182 Matsuo, J. Fukushima, Y. Fukasawa, Y. Tani, Y. Taketani, H. Uchino, J.Y. Kim, J.
1183 Inatomi, I. Okayasu, K. Miyamoto, E. Takeda, T. Goya, and H. Endou. 2001.
1184 Human L-type amino acid transporter 1 (LAT1): characterization of function and
1185 expression in tumor cell lines. *Biochim Biophys Acta*. 1514:291–302.
1186 doi:10.1016/s0005-2736(01)00384-4.

1187 Yu, L., L. Wang, and S. Chen. 2010. Endogenous toll-like receptor ligands and their
1188 biological significance. *J Cell Mol Med*. 14:2592–2603. doi:10.1111/j.1582-
1189 4934.2010.01127.x.

1190